Engineering Structures 345 (2025) 121536

Contents lists available at ScienceDirect

Engineering Structures

journal homepage: www.elsevier.com/locate/engstruct

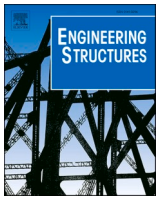

Experimental investigation into cracking in edge restrained concrete walls

Karim El Khoury [a], Robert Vollum [a,*], Bassam Izzuddin [a], John Forth [b]

[a] Department of Civil and Environmental Engineering, Imperial College London, UK
[b] School of Civil Engineering, University of Leeds, UK

ARTICLE INFO

Keywords:
Reinforced concrete design
Edge restraint induced cracking
Experimental investigation
Large scale walls

ABSTRACT

The paper describes an experimental investigation into cracking in edge-restrained reinforced concrete walls cast onto concrete bases. The aim of the investigation was to study the mechanics of cracking in relatively thin edge-restrained walls (< ~ 500 mm) in which through thickness temperature variations due to heat of hydration can be neglected. Twelve walls, each 5.2 m in length, but with varying thickness, height, concrete mix design, reinforcement, and formwork insulation were monitored over a period of at least 3 months. Detailed measurements were made of the temperature rise during heat of hydration, strain and crack width. The paper describes the experimental results in detail, including the development of cracking with time. The measured restrained strains, time of cracking and crack widths are compared with those calculated with EC2–04, EC2–23 and Ciria Report C766 which all adopt the same unrealistic model for calculation of crack width. EC2–04 gives the greatest crack widths and C766 the least due to the lower adopted restraint factor. Significantly, C766 was found to greatly underestimate the maximum measured crack widths with EC2–04 and EC2–23 providing more realistic estimates. Based on the observed cracking behaviour, the paper proposes a simplified mechanical model for the calculation of crack width in relatively thin edge-restrained walls.

1. Introduction

After the hydration phase [1], concrete structures undergo early age (EA) thermal contraction followed by autogenous and drying shrinkage in the longer term [2]. Typically, members are restrained from contracting freely, resulting in restrained strain— the portion of free strain that is prevented from materialising. This restrained strain induces tensile stress that leads to cracking if the tensile resistance of concrete is exceeded. Restraint to volumetric changes can be internal or external [2,3]. Internal restraint is caused by reinforcement [4] as well as thermal gradients within the section, arising from the core heating more than the surface during the hydration phase [2] and subsequent differential shrinkage [5]. External restraint develops when a member is cast against a more mature rigid support and is classified as edge, end, or a combination of the two [6]. Internal restraint is mostly applicable to very thick members while external restraint dominates in relatively thin elements [2,7] which are the focus of this research. Control of cracking in edge-restrained members is governed by the reinforcement parallel to the restrained edge and is less well understood [8,9] than cracking in end restrained members [5]. Recently, Schlicke and Matiašková [10] have made major theoretical contributions to the determination of restraint induced stress, and crack width, in thick base restrained walls where the risk of cracking is best assessed with coupled thermo-chemo-mechanical models [3]. Schlicke and Matiašková considered geometries in which the ends of the base and wall are free to lift, thereby introducing curvature into the wall. This study examines the alternative case of cracking in relatively thin edge-restrained walls (< ~500 mm), where through thickness temperature variations due to heat of hydration can be neglected. The study considers walls that are constrained to remain straight [11] by the base slab.

Early age thermal and long-term shrinkage strain are usually insufficient to cause a fully developed crack pattern to form in both end and edge restrained members [12]. Otherwise, the behaviour of end and edge restrained members is fundamentally different due to the tensile force being uniform along the length of end restrained members [5] but not edge restrained members [6]. In end restrained members, the axial force drops throughout the member length each time a crack forms due to the reduction in axial stiffness [5]. Consequently, tension develops in a saw-tooth fashion as the free strain increases, with the peak force being equal to the cracking load. The crack width in end restrained members can be calculated from consideration of equilibrium and strain compatibility in terms of the current number of cracks and free strain

* Corresponding author.
E-mail address: r.vollum@imperial.ac.uk (R. Vollum).

https://doi.org/10.1016/j.engstruct.2025.121536
Received 4 April 2025; Received in revised form 1 October 2025; Accepted 7 October 2025
Available online 15 October 2025

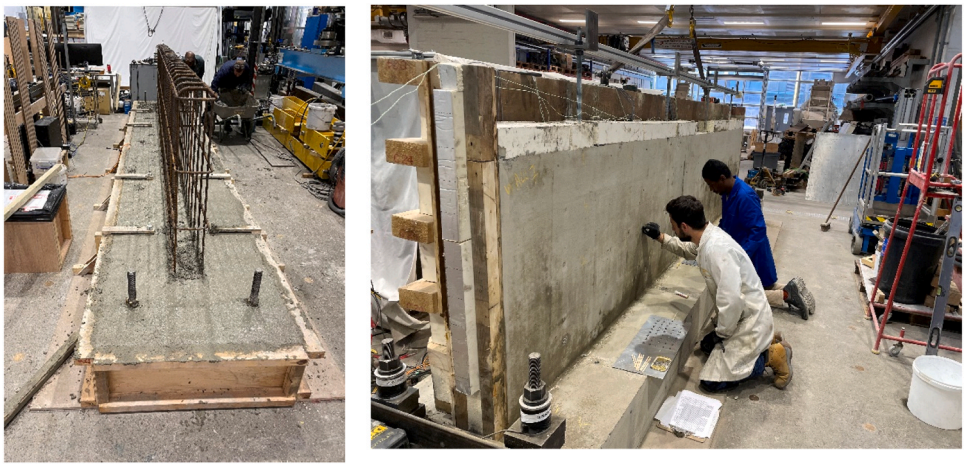

Fig. 1. Construction of wall specimens: a) following casting of base and b) fixing DEMEC points.

[5]. As done in European practice [13,14,15], it is simpler to calculate the maximum crack width which arises under the cracking load, just before the next crack forms. The behaviour of edge restrained members is more complex since the degree of restraint, and hence tensile stress, varies both spatially within the member and during construction as successive pours are cast. In edge restrained members, cracking only relieves stress locally to either side of the crack, unlike end restrained members. Codes typically calculate the crack width in edge restrained members as the product of the crack spacing and the crack-inducing strain. The latter depends on the restrained part of the imposed strain and the extensibility of the concrete, which is related to its tensile strain capacity [16]. The restrained strain is normally calculated in design codes [16] as the product of a restraint factor and the free strain. Differences arise between design standards in the calculation of both the restraint factor and crack spacing. For example, BS EN 1992 [13] allows the restraint factor for edge restrained walls to be taken as either 0.5 or estimated with linear elastic finite element analysis. Alternatively, C766, ACI 207.2 [17] and ACI 224 [18] provide formulae for calculating the variation in restraint factor over the wall height.

At the time of writing, the principal documents used in the UK for the assessment of cracking in edge-restrained members are BS EN 1992–1–1 (2004) [13] (depicted EC2–04), BS EN 1992–3 (2006) [14] (depicted EC2–06), and C766 [2]. The latter provides non-contradictory complementary guidance to BS EN 1992. BS EN 1992–1–1 (2023) [15] (depicted EC2–23) has recently been published and will, in due course, supersede BS EN 1992 (Parts 1 (2004) and 3 (2006)), which will be withdrawn in 2028. Previous work [8,19,20] suggests that current UK guidance may not properly model cracking in edge-restrained elements. For example, Jędrzejewska et al. [20] found restraint-induced crack widths to exceed crack widths calculated with EC2–04 and C766 in numerous structures on multiple occasions. They concluded that a re-evaluation of design guidance is required, with C766 most pressing as it predicts lower crack widths than EC2–04. EC2–23 proposes several changes to the EC2–04 guidance on edge-restraint cracking that are mostly in line with C766.

To address these issues, 12 edge restrained walls were tested in the Structures Laboratory at Imperial College London (ICL) as part of an EPSRC funded investigation into restraint induced cracking. This was a joint project with the University of Leeds (UoL) who also tested walls with similar geometry [21] but without achieving early age cracking. The present research was undertaken in response to concern within the UK construction industry that the then current UK design guidance [2], [13] was inadequate to control restraint induced crack widths in edge restrained walls. The research hypothesis is that cracking in thin edge restrained walls is not well modelled by current practice [2,13,14,15] which 1) calculates crack width in terms of the restrained strain in an uncracked member and 2) takes the crack spacing as that in a tie in which stabilized cracking has developed [2,13]. Neither of these assumptions is realistic. Recent laboratory and field investigations into the predictive capacity of the new Annex D method in EC2–23 have similarly highlighted these challenges [22]. As noted by Jędrzejewska et al. [20], analysis of restraint induced crack widths observed in the field is hampered by missing information of material properties and environmental conditions. The novelty of the walls tested in this project lies in their scale, number and quantity of investigated parameters. The authors are unaware of any other laboratory-based investigations of this scale into restraint induced cracking. Consequently, the comprehensive nature of the investigation makes the results invaluable for future reference, model development and model validation. In this paper, the findings are used to evaluate current international design guidance on restraint induced cracking and make suggestions for their improvement. The key scientific contribution of the paper is to show that there are significant differences between the experimentally observed behaviour and that assumed in the derivation of current design guidance. In particular, the tests show that full height, or near full height, primary cracks spaced at approximately the wall height can develop at EA in edge restrained walls. In this case, the final crack pattern is shown to depend on the interaction between the horizontal reinforcement and the primary cracks. The paper concludes by presenting a simplified mechanically based model for calculating long-term crack widths in walls in which EA thermal cracking occurs. The model, which accounts for the interaction between the horizontal reinforcement and the primary cracks, is shown to give better predictions of maximum crack width in the tested walls that cracked at EA than EC2–04, C766 and EC2–23.

2. Overview of the experimental setup

2.1. Testing programme

The experimental programme at ICL consisted of 12 walls with length of 5.2 m, cast onto bases measuring 6 m long × 0.9 m wide × 0.3 m deep as illustrated in Fig. 1. The dimensions of the wall and base were scaled up from those adopted in a pilot study [19] at the UoL and were chosen to be the largest that could be handled in the laboratory. The wall aspect ratio (L/H where L is the wall length and H the height) was initially chosen to be 4 based on the pilot study at UoL. For water-tight construction a maximum aspect ratio of 3 is commonly recommended [23], but this relates to walls that are sequentially cast against previously cast lengths of wall where the effective aspect ratio is 6 for the most recently cast length of wall. Variables in the tests included wall geometry, reinforcement arrangement and concrete mix design. Two walls were cast without horizontal reinforcement to study the crack

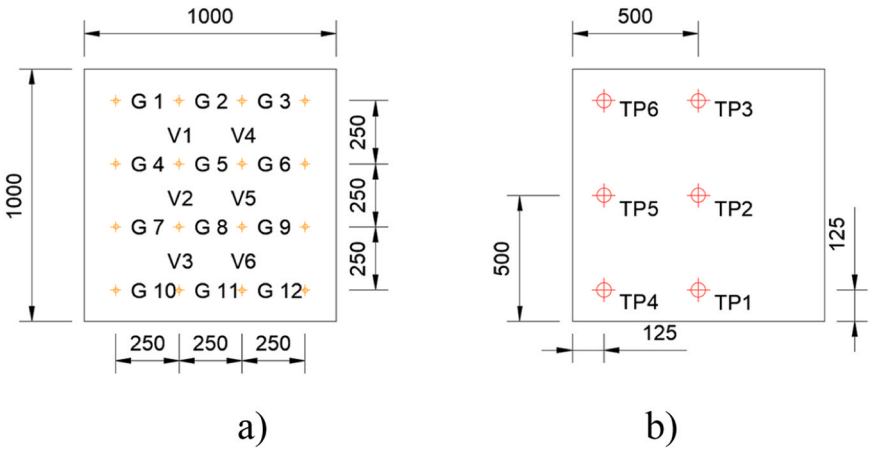

Fig. 2. Location of a) DEMEC points and b) thermocouples in trial panel.

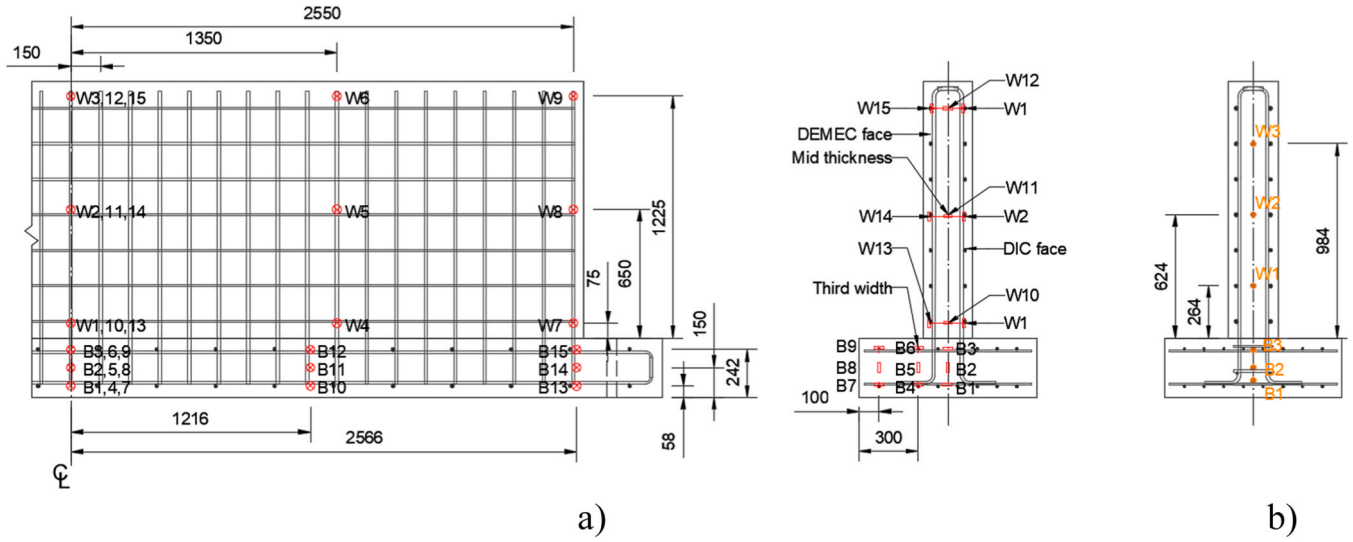

Fig. 3. Typical location in wall of a) thermocouples and b) vibrating wire gauges.

pattern in the absence of horizontal reinforcement. In the remaining walls, the horizontal reinforcement ratio was varied between just below the minimum required by [2] and 1.3 % to study its effect on crack width. The bases were all cured for at least 28 days before casting the wall, which was cast directly onto the base without a kicker as shown in Fig. 1. The joint between the base and wall was roughened with a trowel after casting. Subsequently, it was cleaned and further roughened with a needle scaler before the wall was cast. To prevent curling, each end of the base was bolted down to the laboratory strong floor, just prior to casting the wall, with a pair of holding-down bolts each prestressed to 100 kN. Control specimens were cast alongside each base and wall to determine concrete tensile and compressive strength, modulus of elasticity, shrinkage strain, and creep.

The early age development of concrete compressive strength in the wall was determined from temperature match cured cubes. An unrestrained trial panel (TP) measuring 1×1 m^2 in elevation was cast alongside each wall from W2 onwards. Each TP had the same thickness and formwork insulation as its companion wall. The wall and TP were cast on the same day using concrete from the same batch and stripped at almost the same time the following day ensuring similar exposure conditions for each. The TPs were used to determine the coefficient of thermal expansion (CTE) of the concrete and the shrinkage strain (i.e. sum of drying and autogenous shrinkage) in the TP, which is assumed to be the same as in the companion wall. Knowing the CTE, and shrinkage in the TP, allowed the free strain to be estimated in the companion wall as the sum of the thermal strain, calculated from the temperature change in the wall, and the shrinkage strain in the TP.

Each wall was monitored for at least 3 months during which detailed measurements were taken of temperature, strain and crack width. Concrete surface strains were measured on one side of the wall and trial panel with a DEMEC gauge. Digital image correlation was used to measure strains in the other face of the wall, but these are not reported here due to difficulties in interpretation at early age. Strains in the wall were measured between DEMEC points positioned in a regular rectangular grid with rows of points positioned at vertical centres of 250 mm with the bottom row located 150 mm above the base. Horizontally, DEMEC points were spaced at 250 mm centres within the central 1500 mm of the wall and at 500 mm centres at the wall ends. In the trial panel, DEMEC points were positioned as shown in Fig. 2. Thermocouples were used to monitor temperature variations throughout the wall (see Fig. 3), and trial panel (see Fig. 2), from casting until the end of monitoring (EOM). Other instrumentation, included vibrating wire gauges, positioned at the centreline of the wall, as shown in Fig. 3, measuring strains internally within the concrete and electrical resistance strain gauges (not reported here) measuring reinforcement strain. Crack widths were measured with a crack microscope with measuring resolution of 0.02 mm. Further details of the wall construction and monitoring can be found in [21] and [24].

Table 1
Wall dimensions, mix design, insulation and reinforcement.

Wall	$H \times t$ [mm^2]	$\frac{A_b}{A_w}$	$\frac{L}{H}$	Mix design	Insulation	Reinforcement			
						Horizontal			Vertical
						ϕ in each face @ spacing	ρ_h	Cover [mm]	ρ_v
W1	1300 × 250	0.8	4.0	M1	50 mm PIR	10 mm @ 180 mm	0.3 %	40	1.1 %
W2	1025 × 250	1.1	5.1	M2		16 mm @ 180 mm	0.9 %	25	
W3						16 mm @ 180 mm		25	
W4				M4		10 mm @ 300 mm	0.2 %	30	0.5 %
W5						10 mm @ 180 mm	0.3 %	25	
W6						10 mm @ 300 mm		25	
W7						10 mm @ 180 mm	0.5 %	25	
W8	1025 × 175	1.5				16 mm @ 180 mm	1.3 %	25	
W9				M6	100 mm PIR	16 mm @ 300 mm	0.8 %	25	0.7 %
W10						-	0.0 %	35	
W11	1300 × 175	1.2	4.0			16 mm @ 180 mm	1.3 %	25	
W12						-	0.0 %	25	

Note: H = wall height, t = wall thickness, A_b = cross sectional area of base, A_w = cross sectional area of wall, L = wall length, ϕ = bar diameter, ρ_h = horizontal reinforcement ratio, ρ_v = vertical reinforcement ratio

Table 2
Details of bases and walls mix design.

Mix name	Mix grade	Cement [kg/m^3]	w/c ratio	% fines	Aggregate type	Maximum aggregate size [mm]	Assignment to bases (B) and walls (W)
M1	Prescribed	385	0.45	0.45	Limestone	20	B1 to B2, W1
M2	Prescribed	410	0.60	0.60	Limestone	20	B3, W2 to W3
M3	C30/37	360	0.46	0.48	Limestone	10	B4 to B5
M4	C30/37	361	0.45	0.48	Gravel	10	W4 to W5
M5	C50/60	452	0.37	0.42	Limestone	20	B6 to B12
M6	Prescribed	410	0.56	0.60	Gravel	20	W6 to W12

Note: w/c = water to cement ratio

2.2. Variations to promote early age (EA) cracking

To increase the chance of EA cracking, the wall dimensions, mix design and formwork insulation were modified during the test campaign as shown in Table 1. All these modifications could occur in the field, with the increase in temperature due to added insulation arising in hot weather concreting. All the bases were reinforced, top and bottom, with 12 mm bars at 100 mm spacing longitudinally and 10 mm bars at 300 mm spacing transversely. The vertical reinforcement in each face of the walls consisted of 16 mm diameter bars at 150 mm spacing in walls W1 and W2, and 12 mm diameter bars at 180 mm spacing in walls W3 to W12. The horizontal reinforcement varied as shown in Table 1. Details of the concrete mix designs, including coarse aggregate type, for the bases and walls are presented in Table 2. Limestone coarse aggregate was crushed and the gravel was marine dredged. To maximise the temperature rise during heat of hydration, the plywood formwork was insulated with PIR boards, with thickness of 50 mm or 100 mm, as indicated in Table 1.

Wall W1 did not crack. Consequently, the height of walls W2 to W5 was reduced from 1300 mm to 1025 mm to increase the wall aspect ratio (L/H) from 4.0 to 5.1, and the base-to-wall area ratio (A_b/A_w) from 0.83 to 1.05. These changes increased the restraint provided by the base and hence increased the risk of cracking. The concrete mix design was also modified by increasing the cement content, fines percentage, and

Table 3
Mechanical properties at 1, 3 and 28 days (cured in water at 20 °C).

		1 day	3 days			28 days		
	Mix name	f_{ctm} [MPa]	f_{cm} [MPa]	f_{ctm} [MPa]	E_{cm} [GPa]	f_{cm} [MPa]	f_{ctm} [MPa]	E_{cm} [GPa]
W1	M1	2.0	-	2.5	-	51.8	3.1	35.7
W2	M2	-	-	1.6	-	42.6	2.9	30.9
W3		-	-	2.1	-	42.5	2.8	31.9
W4	M4	1.4	27.9	2.3	-	41.3	2.6	30.5
W5		1.4	21.4	2.0	-	42.2*	2.7	-
W6		2.0	30.2	2.5	35.6	40.9	2.7	37.3
W7		1.4	22.4	1.8	29.8	29.4	2.0	31.4
W8		1.1	21.7	1.6	26.8	33.6	2.2	32.9
W9	M6	1.7	24.6	1.9	32.0	41.6*	2.6*	31.8
W10		1.2	-	-	27.7	34.7	2.6	31.6
W11		1.0	-	-	29.5	31.9	2.6*	33.3
W12		1.4	26.1	2.2	-	34.2	2.8	36.9

Note: f_{ctm}= mean tensile strength, f_{cm} = mean compressive strength, E_{cm} = mean elastic modulus

Table 4
Temperature match cured (TMC) and 20 °C cured concrete cube (100 ×100 ×100 mm^3) strengths.

		1 day		3 days		7 days		28 days	
	Mix name	TMC [MPa]	20 °C [MPa]	TMC [MPa]	20 °C [MPa]	TMC [MPa]	20 °C [MPa]	TMC [MPa]	20 °C [MPa]
W1	M1	-	32.9	-	44.8	-	51.6	-	60.9
W2	M2	29.3	17.2	32.1	27.8	-	-	44.7	44.6
W3		28.6	16.9	30.1	30.8	39.0	37.6	49.0	46.9
W4	M4	25.9	18.4	31.4	30.1	37.2	36.1	40.1	45.3
W5		25.7	12.7	36.7	31.4	42.3	40.3	-	48.6
W6		39.6	24.5	40.2	38.7	42.2	43.0	53.2	51.2
W7		22.9	14.9	27.6	25.0	30.0	29.6	35.9	37.5
W8		19.5	13.0	25.5	22.7	-	-	37.2	36.6
W9	M6	27.8	14.2	25.9	26.8	37.9	34.5	-	44.2
W10		19.4	11.8	-	-	-	-	28.3	36.0
W11		19.3	15.2	-	-	30.1	27.9	38.5	38.2
W12		32.5	20.6	25.0	31.5	44.0	41.4	48.1	42.9

water-to-cement ratio to increase the heat of hydration and drying shrinkage. These changes resulted in walls W2 to W3 cracking at 10 days and 7 days respectively. To further promote EA cracking, the aggregate type was changed from limestone to gravel (M4) in walls W4 and W5. Changing the aggregate type to gravel increased the CTE of the hardened concrete from 8.5 to 12.2 $\mu\varepsilon/^{\circ}C$ but owing to a drop in peak temperature T_1, first cracking occurred at 19 and 20 days respectively. In walls W6 onwards, the wall thickness was reduced to 175 mm, and the mix design changed to M6 with gravel aggregate. To maximise differential strain, the base of wall W6 onwards was cast from M5 with limestone aggregate. The thickness of the insulation to the formwork was also doubled to 100 mm. These changes led to EA thermal cracks forming in walls W6 onwards. The wall height was increased to 1.3 m in W11 and W12 to study the effect on EAT cracking of reducing the wall aspect ratio from 5.1 to 4.0.

3. Experimental results

Concrete compressive and tensile strengths were obtained in line with BS EN 19390–3 [25] and elastic modulus according to BS EN 19390–13 [26]. Concrete compressive strength (f_{cm}) was determined from 100 mm diameter cylinders while tensile strength (f_{ctm}) was taken as 90 % of the measured 150 mm diameter split cylinder strength [13]. Table 3 gives the resulting mechanical properties for specimens cured at 20 °C while Table 4 gives strengths for the temperature match cured cubes (TMC) and companion control cubes cured in water at 20 °C. When not tested at exactly 28-days (depicted * in Table 3), the 28-day strength was determined through interpolation using equations 3.1 and 3.4 from EC2–04 (Eqs. (1) and (2) below) for strength development in compression and tension respectively.

$$f_{cm}(t) = \beta_{cc}(t) f_{cm} \tag{1}$$

in which

$$\beta_{cc}(t) = \exp\left\{ s\left[1 - \left(\frac{28}{t}\right)^{1/2}\right]\right\}$$

where f_{cm} is the mean compressive strength at 28 days, t is the concrete age in days and $s = 0.2$ for cement classes CEM 42.5 R, CEM 52.5 N and CEM 52.5 R.

$$f_{ctm}(t) = (\beta_{cc}(t))^{\alpha} f_{ctm} \tag{2}$$

where f_{ctm} is the mean tensile strength of concrete at 28 days, $\alpha = 1$ for $t < 28$ and $\alpha = 2/3$ for $t \geq 28$.

Eqs. (1) and (2) are also adopted in EC2–23 where they are depicted B.2 and B.3. In EC2–23, s is replaced with s_c, which is assumed to depend on the concrete strength and class, and $\alpha = 0.6$. For Class CN concrete, as adopted in this project, $s_c = 0.5$ for $f_{ck} \leq 35$ MPa and $s_c = 0.4$ for $35 < f_{ck} < 60$ MPa.

As indicated in Table 5, the temperature typically peaked around 20 h after casting following which the formwork was removed with the shuttering first removed on the side that DEMEC points were fixed. Typically, the first set of DEMEC readings was taken within one hour of the peak temperature being recorded. Table 5 also gives the maximum temperature drop (T_1) from peak to ambient at 3 days, shrinkage strain in the TP at EOM and maximum total free strain at 3 days and EOM. The

Table 5
Ambient conditions and components of free strains.

		Mean ambient conditions		Peak temperature drop in walls			Measured shrinkage strain in TP at EOM		Maximum total free strain in wall $\varepsilon_{free} = \varepsilon_{cs} + \alpha_c T_{1,EOM}$	
	Mix name	RH [%]	T [°C]	Age [hrs]	T_1 [°C]	$T_{1,EOM}$ [°C]	Age at EOM [days]	Measured shrinkage ε_{cs} [$\mu\varepsilon$]	3 days [$\mu\varepsilon$]	EOM [$\mu\varepsilon$]
W1	M1	46.6	20.3	18.0	34.9	40.6	112	212†	323	555
W2	M2	39.6	21.7	17.9	34.7	31.3	88	342	303	599
W3		45.5	22.9	17.6	40.5	38.8	78	297	242	624
W4	M4	46.2	21.9	20.9	30.7	33.5	94	208	397	601
W5		45.0	20.4	22.1	30.0	31.8	118	243	389	600
W6		49.5	23.3	20.8	43.9	39.0	111	406	552	875
W7		51.2	24.7	20.4	36.8	40.1	113	463	458	942
W8		39.3	22.1	21.4	32.1	31.8	93	476	382	864
W9	M6	36.4	22.6	21.1	31.7	33.4	94	503	437	892
W10		43.7	24.7	21.7	32.3	29.8	109	656	455	1015
W11		44.5	21.7	21.2	32.5	36.1	252	465	422	877
W12		43.3	20.1	20.3	37.6	41.4	167	458	513	951

Note: RH = relative humidity, T_1 = drop in temperature from peak to ambient at 3 days, $T_{1,EOM}$ = drop in temperature from peak to ambient at EOM, ε_{free} = free strain, ε_{cs} = shrinkage strain, α_c = CTE

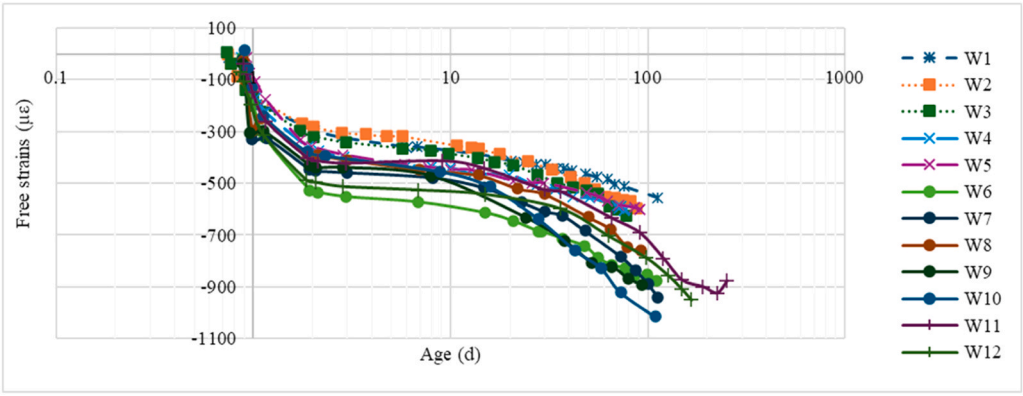

Fig. 4. Experimentally derived maximum free strain calculated from peak temperature.

free shrinkage strain was assumed to be the same in the wall as its corresponding TP since both had the same thickness and ambient conditions. In wall panel W1 without a TP, shrinkage (depicted † in Table 5) was estimated using EC2–04 which gave good estimates of shrinkage in the control specimens. The EA thermal strain was estimated at each set of DEMEC points as the product of the CTE and the measured temperature drop T_1 from peak.

The CTE was determined in two ways. First, it was derived from the temperature drops and corresponding strains measured in the TPs during the first week. The CTE was derived for concrete mix M2 from TP2 to TP3, for M4 from TP4 to TP5 and for M6 from TP6 to TP12. The peak temperature drops were similar in both the TPs and companion walls, but temperatures were spatially less uniform in the walls due to heat being lost into the concrete base. The temperature dropped from peak to ambient over the first 2 days following casting. Shrinkage is estimated to have accounted for only 2–3 % of the measured strain during this period. Consequently, the derived CTE is relatively insensitive to shrinkage over this period. The CTE was also estimated from strain measurements made on heated concrete prisms measuring 150 mm square by 300 mm long with an embedded thermocouple and vibrating wire gauge. Strains were also measured on each face of the prism with a DEMEC gauge with a gauge length of 250 mm. These tests were carried out for concrete from base B5 with limestone coarse aggregate and walls W4 and W5 with gravel aggregate. The specimens were heated in a water bath from room temperature to 60°C in increments of around 15°C. The CTE was determined from strain measurements taken at each temperature interval. The prism tests gave CTE of 12.2 με/°C for concrete with gravel aggregate (W1 to W5) and 8.5 με/°C for concrete with limestone aggregate (W6 to W12). These values are almost the same as the mean values of 12.3 με/°C and 8.5 με/°C obtained from the TP. Consequently, the CTE was taken as 12.2 με/°C for concrete with gravel aggregate (W1 to W5) and 8.5 με/°C for concrete with limestone aggregate (W6 to W12).

Fig. 4 shows the variation with time in the maximum free strain calculated in each wall from the time of peak temperature until EOM. In the calculation of free strain, the thermal strain was calculated as the product of the maximum temperature drop in the considered wall and the CTE, while the shrinkage strain was obtained from a line of best fit placed through the shrinkage strains measured in the corresponding TP. Graphs with the same line and marker type depict geometrically similar walls cast from the same mix design. Even though walls W4 to W5 developed higher EAT than walls W2 to W3, subsequent shrinkage strain was less, resulting in similar final free strains for walls W1 to W3 and W4 to W5. Fig. 4 shows that by the end of monitoring, free strains in walls W6 to W12 were around double that in wall W1.

Table 6
Summary of first crack formation in walls W2 to W12.

Wall	Age [hrs] from end of casting	At first cracking		Max Width [mm]	Crack end height from base [mm]		Location
		$\varepsilon_{free,max}$	$\varepsilon_{rest,max}$		h_{bottom}	h_{top}	
1	No cracks						
2	247	353	75	0.10	225	260	Central
3	175	373	85	0.04	394	431	Central
4	468	467	114	0.02	320	360	Central
5	487	490	121	0.02	250	515	End: at opening
6	27.4	322	94	0.02	270	510	Central
7	28.1	325	66	0.04	100	680	Central
8	47.5	385	125	0.02	130	610	Central
9	45.8	429	116	0.04	160	610	Central and ends
10	45.8	379	322	0.38	20	1025	Central
11	45.4	401	118	0.04	290	610	Central
12	44.4	487	93	0.14	130	1150	Central

3.1. Initial cracking behaviour

The time of first cracking (in hours from end of casting), initial crack length and crack width are summarised for all walls in Table 6, which also shows the maximum measured free ($\varepsilon_{free,max}$) and restrained ($\varepsilon_{rest,max}$) strains at first cracking. Average restrained strains (i.e. difference between free and measured strain) were calculated for each row of DEMEC points over the 1) central 1.5 m and 2) two end lengths of 1.5 m. The maximum restrained strain was taken as the greatest of these averages, which typically occurred near mid-height of the wall within the central 1.5 m. First cracking occurred in walls W2 to W5 between 10 and 20 days after casting due to the combined effect of EAT contraction and shrinkage, but in walls W6 to W12 on day 2 due to EAT contraction. None of the trial panels ever cracked, confirming that cracking in the walls was due to restraint. Fig. 5, which is drawn to scale, shows the initial crack pattern and crack widths in walls which cracked at EA while Fig. 6a shows the crack in wall W6 at first formation. The width of through cracks differed in each face of the wall as illustrated in Fig. 6b, which shows the variation in crack width in a core extracted from wall W8 at EOM. Following removal of the core, the crack partially closed but the variation in width is still visible. As shown in Fig. 5, EA cracking first occurred in the central part of the wall with the centre of the crack located between 24 % and 40 % of the wall height above the top of the base. A few minor cracks were detected in the top of the base, from early age, but these were only recorded for bases B4 to B12. The EA cracks tended to be through cracks that extended and widened in the first few days after forming. As shown in Fig. 7, cracks that formed within the first 3 days were spaced at approximately the wall height. Subsequently,

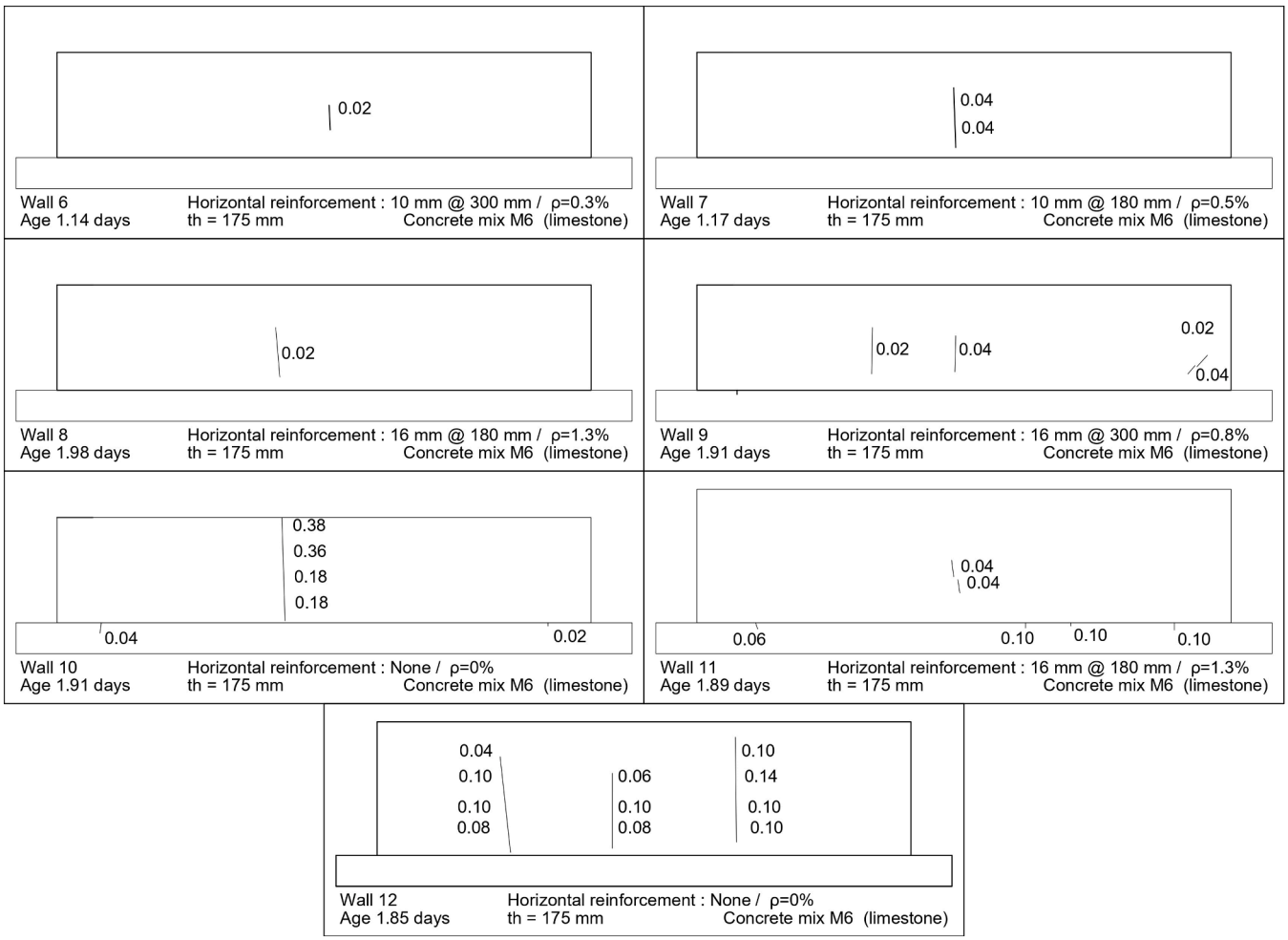

Fig. 5. Crack patterns in W6 to W12 on day of first cracking (crack width in mm).

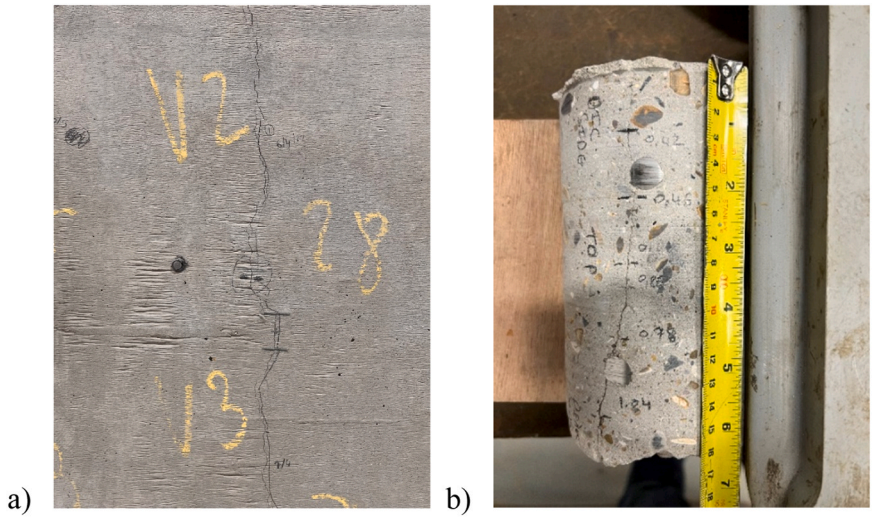

Fig. 6. Crack in a) W6 at first formation and b) through thickness of core extracted from W8 at EOM.

narrow shorter cracks subsequently formed in between the EA cracks as indicated in Fig. 7. Cracks that formed at EA tended to be longer and wider at EOM than cracks which formed later. The maximum initial EA crack width in walls W6 to W9 and W11 was 0.04 mm. By day 3, three well defined cracks had formed in wall W6 and W7 with maximum widths of 0.14 and 0.10 mm, respectively. In wall W10, without horizontal reinforcement, the initial crack was full height when first observed with a maximum width of 0.38 mm. In wall W12, three almost full height through-cracks developed almost simultaneously with initial width between 0.04 and 0.14 mm.

3.2. Long-term cracking

Two types of cracking behaviour were observed over the monitoring period as described below:

1. In walls W2 to W5, following first cracking between 7 and 20 days after casting, evenly distributed short surface cracks developed with maximum width of 0.10 mm.
2. In walls W6 to W12, following EA cracking within 2 days of casting, narrow shorter cracks formed in between the EA cracks as indicated

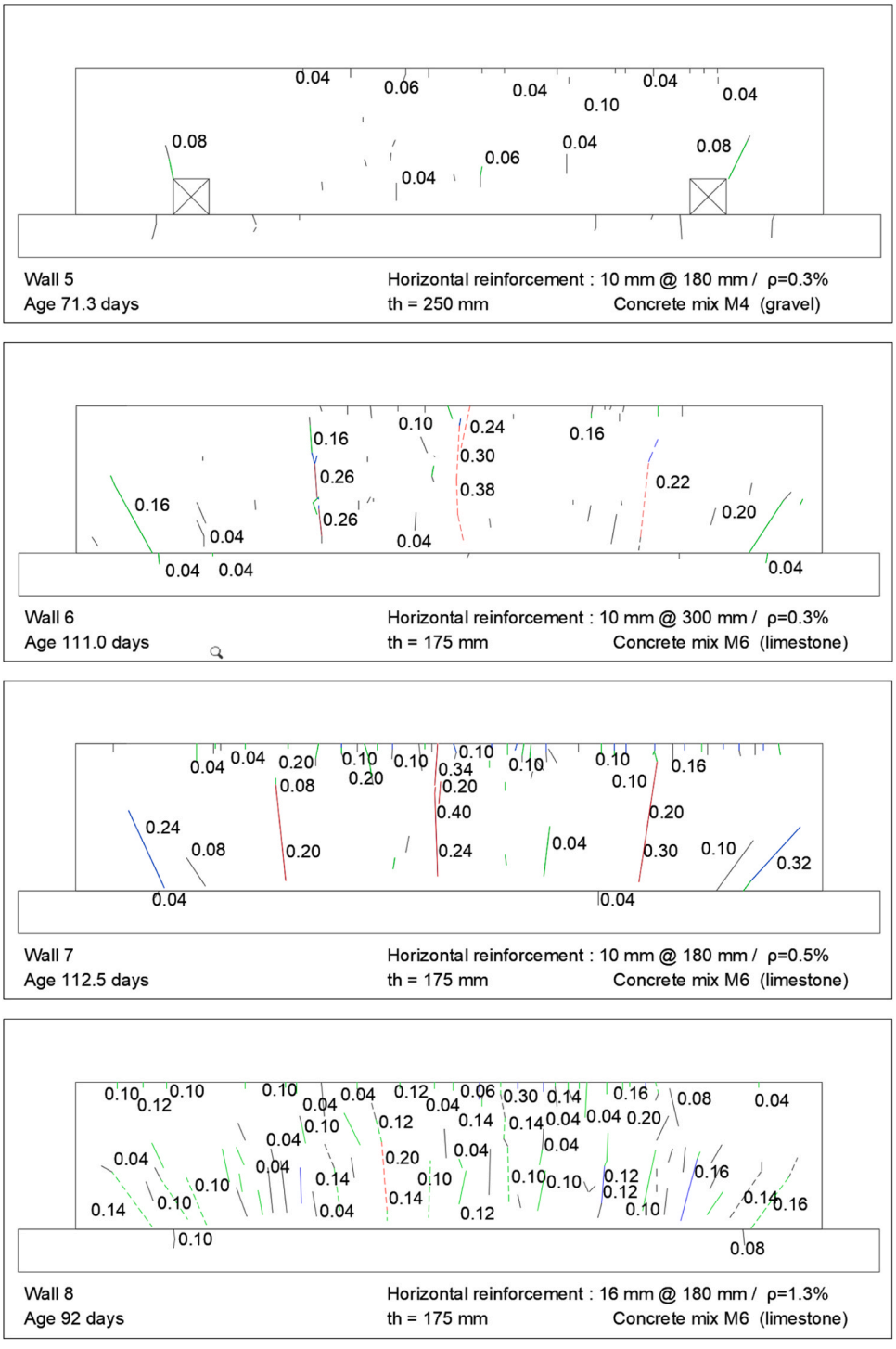

Fig. 7. Crack patterns in walls W5 to W12 at end of monitoring (crack width in mm) (cont.).

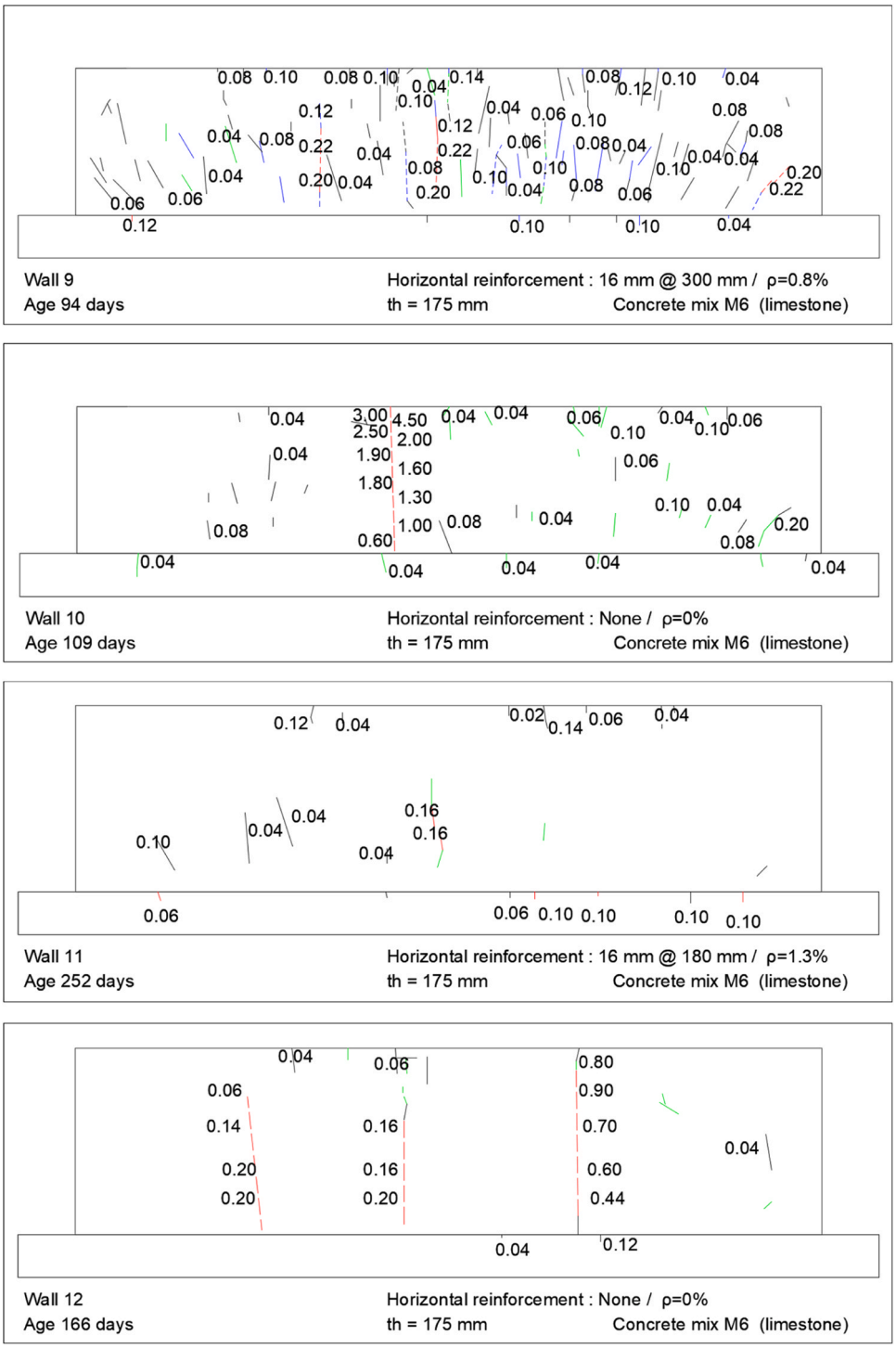

Fig. 7. (*continued*).

in Fig. 7 which, like Fig. 5, is drawn to scale. Cracks that formed at EA tended to be longer and wider than cracks which formed later.

By EOM, all walls except W1 had cracked as indicated in Table 7 which summarises the maximum observed crack width in each wall and its location. The final crack patterns in walls W5 to W12 are shown in Fig. 7, where cracks are colour coded, as indicated in the legend, according to when they formed. Cracking in walls W2 to W4 was similar to W5. Known through-cracks are shown with a dashed line. Maximum crack widths typically occurred in the central region of walls. Cracks in walls W2 to W5 were relatively short, narrow, and closely spaced (see wall W5 in Fig. 7). The cross-hatched squares in the elevation of wall W5

Table 7
Summary of maximum crack widths at final measurement in walls W2 to W12.

Wall	ε_{free} με	$\Delta\varepsilon_{base}$ με	Age [days]	Crack width [mm]	$\frac{h_{max\ width}}{H}$	Region of wall
2	599	3	87	0.12	26 %	Central
3	624	101	69	0.10	22.0 % 36.9 %	Central End: At the corner of the end opening
4	601	99	69	0.10 0.06	41–44 % 93 %	End: At the corner of the end openings End
5	600	102	71	0.10	94 %	Central
6	875	18	111	0.38	40 %	Central
7	942	116	112	0.40	51 %	Central
8	864	67	92	0.30	94 %	Central
9	892	85	94	0.22	41 %	Central
10	1015	36	109	4.50	94 %	Central
11	877	157	252	0.16	35 %	Central
12	951	73	166	0.90	75 %	Central

Note: $\Delta\varepsilon_{base}$ = increase in shrinkage strain in base measured from just before casting wall, $h_{max\ width}$= height above base of maximum crack width.

depict openings that were cast into the wall to allow it to be loaded in direct tension, through a pair of axially loaded struts bearing on cross members threaded through the opening, at the end of the test [27]. In walls W6 to W12, where through-cracks developed at EA, cracks were wider and longer. The maximum final crack width varied between 0.10 and 0.12 mm in walls W2 to W5, which first cracked at 10, 7, 19 and 20 days respectively, but exceeded 0.20 mm in walls W6 to W10 and W12. In walls W6 and W7, the widest cracks were full height and spaced roughly 1 m apart. In walls W8 to W9, the widely spaced primary through-cracks are less evident due to the numerous short cracks in between.

Full height through-cracks, which widened with height above the base, formed in walls W10 and W12 without horizontal reinforcement. A single full height crack developed in wall W10 within two days of casting causing the wall to behave like two separate walls from that point. The total free strain in wall W10 was 1015 $\mu\varepsilon$ at EOM. In the absence of restraint, the corresponding shortening of each half of the wall would be around 2.6 mm which is similar to the crack widths of 2.5 mm and 3 mm measured at the top of the wall immediately above and below the maximum recorded crack width of 4.5 mm which, as shown in Fig. 8, was increased locally by spalling of concrete. The maximum crack width was smaller at 0.9 mm in wall W12, in which the free strain at EOM was 951 $\mu\varepsilon$. The main reasons for the smaller crack widths in W12 appear to be that 1) three cracks formed at early age rather than one in wall W10 and 2) only one of these cracks extended over the full height of the wall and only towards the end of monitoring. Consequently, for much of the test the width of the through cracks in wall W12 was restrained by the bridging of the concrete over the top of the crack. The maximum width of the full height crack in wall W12 increased significantly from 0.26 mm at 63 days to 0.6 mm at 98 days, when the crack became full height. In walls W2 to W3, W6 to W7, W9 and W11 cracks were widest below mid-height of the wall, but in walls W4, W5, W8, W10 and W12 they were widest at the top.

3.3. Distribution of crack width and development with time

Table 8 shows the percentage of crack width measurements within the ranges < 0.05 mm, 0.05–0.2 mm, 0.2–0.3 mm and > 0.3 mm, as well as the total number of measurements, for each wall at EOM. For

Fig. 8. Crack measuring ruler used for main crack of Wall 10.

Table 8
Distribution of crack widths (%) at EOM in walls W2 to W12.

Wall	2	3	4	5	6	7	8	9	10	11	12
ρ_h %	0.9	0.9	0.2	0.3	0.3	0.5	1.3	0.8	0	1.3	0
$<$ 0.05 mm	73	82	85	81	72	62	60	60	58	63	48
0.05–0.2 mm	27	18	15	19	15	28	39	36	31	38	32
0.2–0.3 mm	-	-	-	-	11	5	1	4	0	-	20
$>$ 0.3 mm	-	-	-	-	2	5	-	-	11	-	25
No. measurements	73	55	20	26	46	58	80	84	36	16	25
St deviation (mm)	0.03	0.02	0.02	0.02	0.10	0.10	0.06	0.05	0.83	0.05	0.27

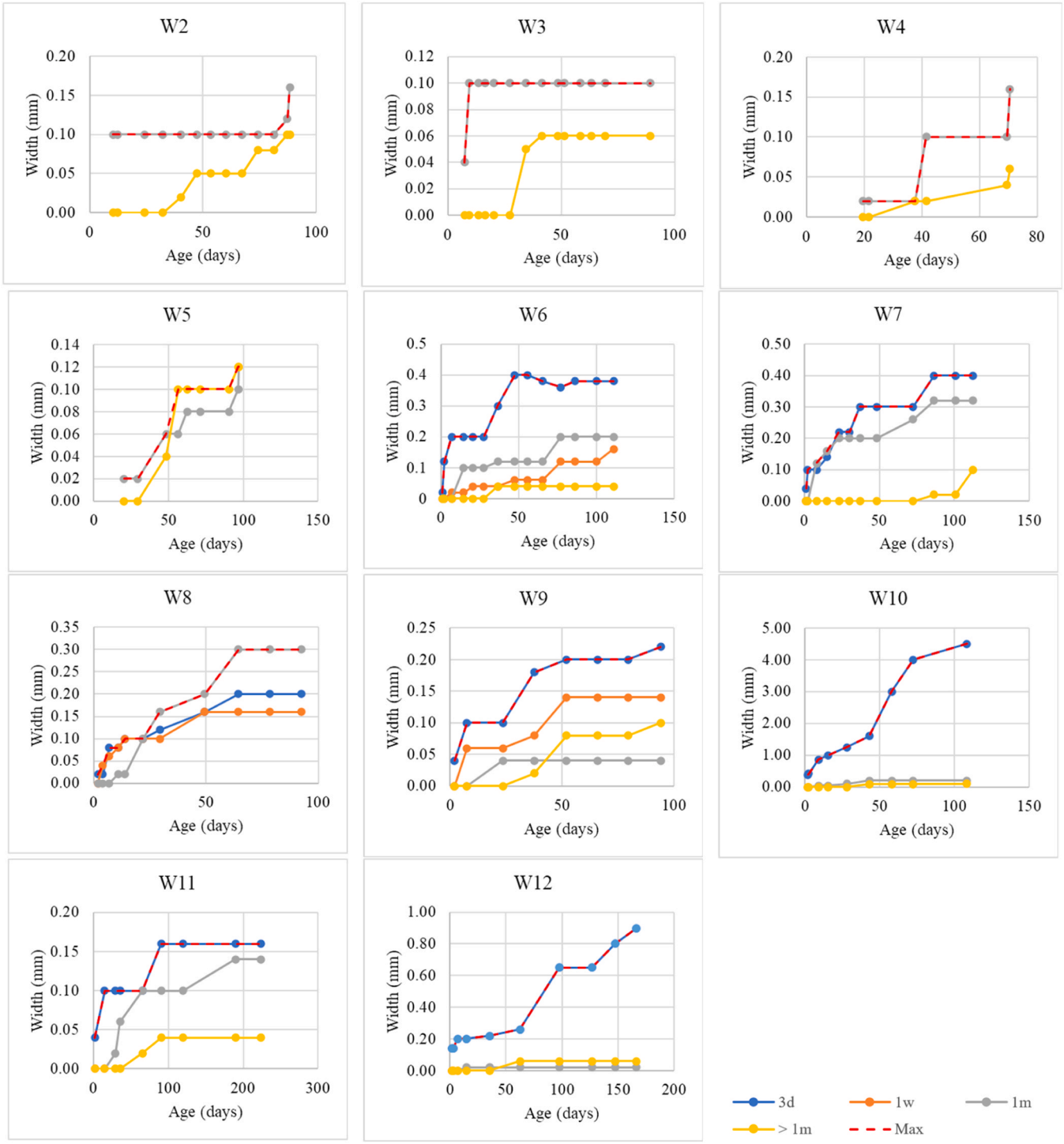

Fig. 9. Development of maximum crack widths with time.

long cracks, like those observed in walls W6 to W10 and W12, several evenly spaced measurements were made along each crack as shown in Fig. 7. Crack widths of 0.05 mm or less, which are not of practical significance [2] were most frequent. For practical purposes, crack widths greater than 0.2 mm are of most concern for water retaining and resisting structures [2]. Table 8 shows that these only developed in walls W6 to W12 where EAT cracking developed.

Cracks that formed earlier tended to be wider than cracks that formed later. This is illustrated in Fig. 9 which shows the variation in crack width with time for the widest cracks that formed 1) within the first three days (3 d), 2) the first week (1 w), 3) the first month (1 m) and 4) later than 1 m (>1 m). The starting point for each interval is the end of the previous interval. In walls W2 to W4, cracks first formed between 7 and 20 days (i.e. in the first month), whereas in walls W6 to W12, the initial cracks formed within the first 2 days of casting. In W6, the widest crack reduced in width beyond 55 days due to a heatwave, which led to a 4.2°C increase in the wall TC readings. Otherwise, cracks tended to widen with time due to the development of shrinkage. When new cracks formed, no noticeable narrowing of existing cracks was observed. Except for W8, in walls that cracked at EA, the widest crack at EOM developed within the first 3 days.

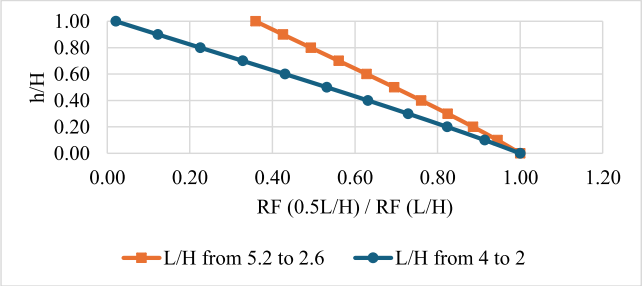

Fig. 10. Reduction in maximum RF when aspect ratio is halved.

4. Assessment of tested walls with EC2-04, C766 and EC2-23

This section evaluates the risk of cracking, and calculates crack widths, in the tested walls with EC2–04, C766 and EC2–23. All three documents calculate the design crack width as:

$$w_k = S(\varepsilon_{sm} - \varepsilon_{cm}) \tag{3}$$

in which S is the maximum, or calculated, crack spacing and $(\varepsilon_{sm} - \varepsilon_{cm})$ is the crack inducing strain which is calculated for edge restraint as follows:

$$\varepsilon_{sm} - \varepsilon_{cm} = R\varepsilon_{free} - k_t\varepsilon_{ctu} \tag{4}$$

in which ε_{sm} is the mean strain in the reinforcement, ε_{cm} is the mean strain in the concrete, R is the restraint factor, ε_{free} is the free strain, k_t is a constant which accounts for tension stiffening provided by concrete between cracks, which is taken as 0 in EC2–04, 0.5 in C766 and 0.4 for long-term cracking in EC2–23, and ε_{ctu} is the tensile strain capacity of the concrete which is increased for creep in C766. R is a restraint factor defined in EC2–23 as:

$$R = 1 - \frac{\varepsilon_{restr}}{\varepsilon_{free}} \tag{5}$$

in which ε_{restr} is the strain which develops in the restrained element (i.e. measured strain). The strain ε_{restr} should not be mistaken for the restrained strain ε_r which is "the component of free strain which is restrained and which generates stresses in the concrete" [2] (i.e. $\varepsilon_r = \varepsilon_{free} - \varepsilon_{restr}$). EC2–23 states that the ratio $\varepsilon_{restr}/\varepsilon_{free}$ may be estimated from elastic analysis allowing for staged construction if relevant. Alternatively, EC2–23, like EC2–06, allows R to be taken as 0.5 for edge restrained walls. C766 gives the expressions below for calculating the restraint factor R in the wall at height h above the base. R is expressed as a multiple of R_j which is the restraint factor at the top of the base at the wall centreline.

$$R_j = \frac{1}{1 + \frac{A_{new}}{A_{old}} \quad \frac{E_{new}}{E_{old}}} \tag{6}$$

$$R = R_j\left[\left(1.372(h/L)^2 - 2.543\left(\frac{h}{L}\right) + 1\right) + 0.044((L/H) - 1.969)(h/H)^{1.349}\right] \tag{7}$$

where A_{new}, A_{old}, E_{new} and E_{old} depict the cross-sectional area and modulus of elasticity of the new (wall) and old (base) sections respectively, L is the wall length and H is the wall height. The restraint factors given by Eqs. (6) and (7) are close to those given by elastic analysis as well as ACI Committee 207 [17].

Consideration of Eq. (7) shows that the restraint factor is greatest at the base of the wall and reduces with height. The height above the base, at which the first crack forms, depends on various factors, including concrete properties, wall aspect ratio, EA temperature distribution, the level of restraint provided by the base, and whether uplift is prevented at the wall ends. According to C766, the restraint factor should be calculated at a height of around $0.1L$ above the base since this is where the widest crack develops. The experimental results from this campaign (see Fig. 7) show this to be a reasonable assumption. The behaviour of walls W10 and W12, without horizontal reinforcement, is explained by the influence of cracking on the restraint factor and subsequent wall deformation. In W10, the central crack separated the wall into two sections with approximate aspect ratio $0.5L/H$. Fig. 10 shows the proportional reduction in the C766 restraint factor R due to L/H halving when a full height crack forms midway along the wall dividing it in two. Reduction factors are plotted against h/H for $L/H = 4$ and $L/H = 5.2$. The restraint factor is seen to reduce significantly, with height h above the base, when L/H halves. In the tested walls, the peak temperature rise was greatest in the top half of the wall due to heat being lost to the base [21], [24]. Consequently, in the case of walls W10 and W12, the reduction in $R\varepsilon_{free}$ due to full height cracking at EA was sufficient to prevent further consequential cracking developing in the walls over the long-term.

4.1. Determination of free strain with EC2-06, C766 and EC2-23

The free strain is the sum of thermal and shrinkage strains in an unrestrained element. The early-age thermal strain materialises within the first three days [21], [24], [28] in non-massive structures such as the walls tested in this study [3]. The difference between the peak temperature and the ambient temperature at 3 days is depicted T_1. Both EC2 and C766 use the full temperature drop T_1 from peak to ambient to calculate restrained strain. This is conservative since compressive stress is induced in the restrained element during the heating phase with the restrained stress subsequently reversing sign and becoming tensile as the wall cools. In the long-term, the restrained strain is increased by shrinkage and drops in ambient temperature below that at 3 days which is the reference time for T_1. EC2–06 calculates the EA and LT restrained strain as follows, where α_c is the CTE for concrete, ε_{ca} is the autogenous shrinkage, ε_{cd} is the drying shrinkage and T_2 the difference between the ambient temperature at 3 days and the minimum likely element temperature.

$$\varepsilon_{rEC2-06EA} = [\alpha_c.T_1 + \varepsilon_{ca}(3)]R \tag{8}$$

$$\varepsilon_{rEC2-06LT} = [\alpha_c(T_1 + T_2 + \varepsilon_{ca} + \varepsilon_{cd}]R \tag{9}$$

As shown below in Eqs. (10) and (11), C766 refines the calculation of restrained strain by introducing EA (3 days) and long-term (≥28 days) creep factors of $K_{c1} = 0.65$ and $K_{c2} = 0.5$ as well as restraint factors R_1, R_2, and R_3 which allow for changes in boundary conditions over time and, hence, restraint.

$$\varepsilon_{rC766EA} = K_{c1}[\alpha_c.T_1 + \varepsilon_{ca}(3)]R_1 \tag{10}$$

$$\varepsilon_{rC766LT} = \varepsilon_{rC766EA} + K_{c1}[(\varepsilon_{ca}(t) - \varepsilon_{ca}(3)) + \alpha_c.T_2]R_2 + K_{c2}.\varepsilon_{cd}.R_3 \tag{11}$$

C766, and EC2–23, define R_1 as the restraint factor corresponding to the boundary conditions after concreting, R_2 as the restraint factor corresponding to the boundary conditions when the maximum temperature drop occurs and R_3 as the boundary condition prevalent during the development of drying shrinkage. Unlike EC2–04, C766 calculates the restrained strain in terms of the differential free strain between the restrained and restraining elements rather than the free strain in the restrained element. Based on Scandinavian practice, EC2–23 assumes by default that only 90 % of the peak temperature drop causes tensile stress

Table 9
C766 max restraint factors at h= 0.1 L (without reduction for creep).

Wall	W1	W2-5	W6-10	W11-12
EA	0.41	0.46	0.52	0.48
LT	0.35	0.39	0.46	0.41

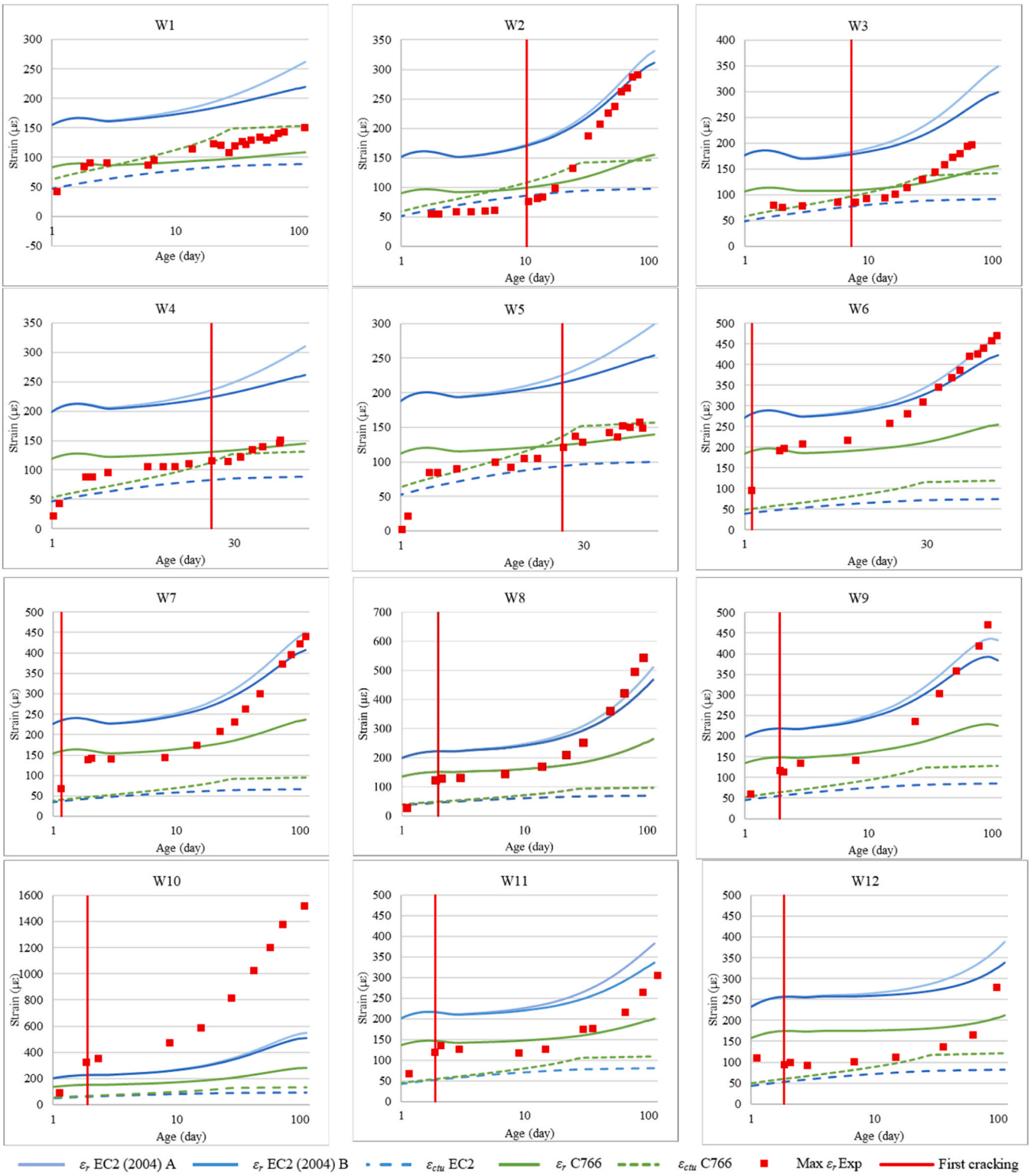

Fig. 11. Restrained stains vs tensile strain capacity for EC2–04 and C766.

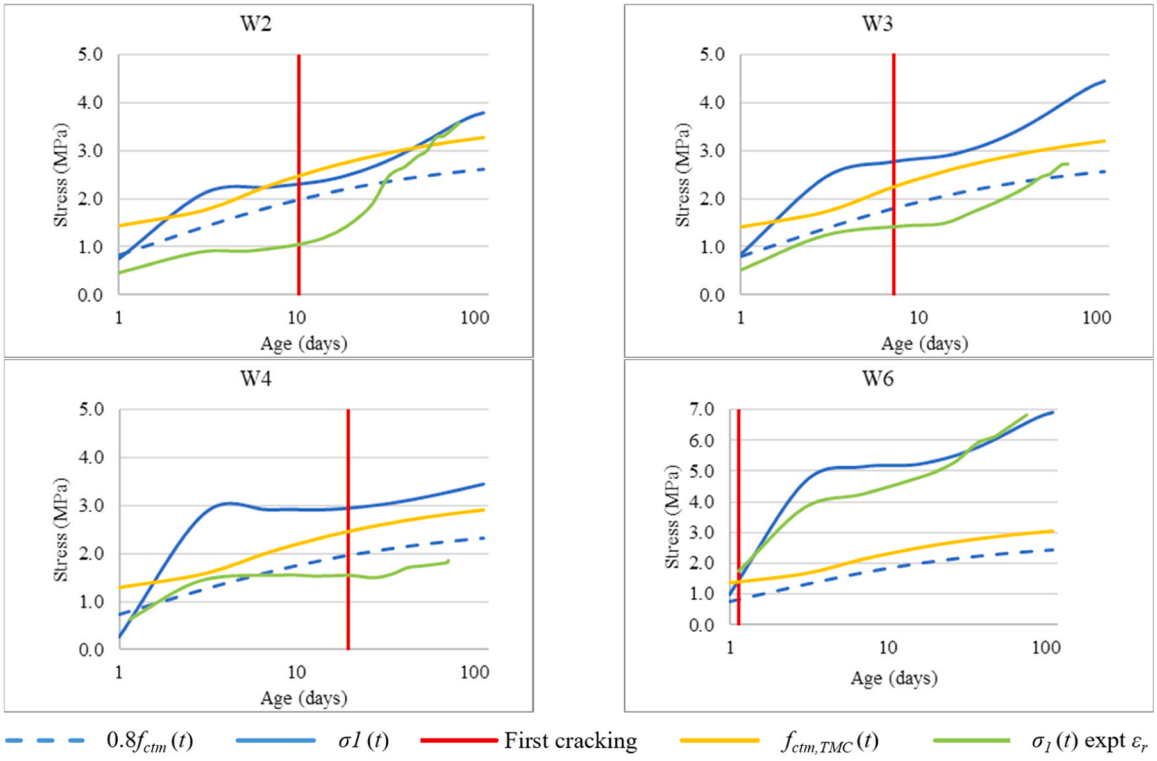

Fig. 12. Restrained stress vs tensile capacity for EC2–23.

as the element is initially in compression and needs to be decompressed before developing tensile stress [29]. Consequently, the thermal drop is defined in Eqs. (12) and (13) below as $k_{\text{Temp}}(T_{\text{c,max}} - T_0)$, where $T_{\text{c,max}}$ is the maximum temperature in the concrete, T_0 the temperature in the restraining element and $k_{\text{Temp}} = 0.9$. Thermal equilibrium with the restraining structure is achieved at t_{crit} which is the most unfavourable time for early age cracking. Time t_2 is the zero-stress instance at which stress switches from compression to tension at the critical section as well as the reference time for development of autogenous (ε_{cbs}) and drying (ε_{cds}) shrinkage. According to EC2–23:

$$\varepsilon_{rEC2-23EA} = R_1\left(k_{\text{Temp}}\alpha_c\left(T_{\text{c,max}} - T_0\right) + \left[\varepsilon_{\text{cbs}}(t_{\text{crit}}) - \varepsilon_{\text{cbs}}(t_2)\right]\right) \tag{12}$$

$$\varepsilon_{rEC2-23LT} = R_1\left(k_{\text{Temp}}\alpha_c\left(T_{\text{c,max}} - T_0\right) + \left[\varepsilon_{\text{cbs}}(t) - \varepsilon_{\text{cbs}}(t_2)\right]\right) + R_2\alpha_c T_2 + R_3\left[\varepsilon_{\text{cds}}(t) - \varepsilon_{\text{cds}}(t_2)\right] \tag{13}$$

4.2. Evaluation of risk of cracking

The risk of cracking in the tested walls was evaluated in accordance with EC2–06, C766 and EC2–23 using the experimentally determined free strains. The code recommended restraint factor of 0.5 for base restrained walls, which makes allowance for creep, was adopted in EC2–06 and EC2–23. In the C766 analysis, restraint factors were determined at a height of 0.1L above the base, as recommended [2], using Eqs. (6) and (7). As shown in Table 9, the resulting restraint factors are around 0.5 before reduction for creep (i.e. putting $K_{c1} = K_{c2} = 1.0$ in Eqs. 10 and 11).

Fig. 11 compares the maximum experimental restrained strain ($\varepsilon_r = \varepsilon_{free} - \varepsilon_{meas}$), calculated as described in Section 3.1, with that calculated with EC2–06 (Eqs. (8) and (9)) and C766 (Eqs. (10) and (11)) using the maximum experimentally determined EAT and shrinkage strains. The shrinkage strain in the wall was assumed to equal that in the companion TP as described in Section 2.1. The time at which cracking was first observed is also shown in Fig. 11, where "EC2 A" and "EC2 B" depict the restrained shrinkage strain calculated in terms of 1) the full shrinkage strain in the wall and 2) the differential shrinkage strain between the wall and base. Fig. 11 shows that earlier than 3 days, C766 tends to overestimate the restrained strain and hence risk of cracking in walls W1 to W5. Subsequently, C766 predicts the experimentally determined restrained strain reasonably well until at least first cracking. In walls W2 and W6 to W12 that cracked significantly, C766 significantly underestimates the LT experimental restrained strain because of cracking causing a localised tensile strain increment within each DEMEC gauge length l (i.e. 250 mm over the central part of the wall) intersected by a crack of $\delta\varepsilon = w/l$ in which w is the crack width. C766 gives better estimates of the measured restrained strain in walls W3 to W5 since only minor cracking occurred in these walls at EOM making the strain increment $\delta\varepsilon = w/l$ small. The increase in restrained strain following cracking is particularly pronounced in wall W10, without horizontal reinforcement, where a single very wide crack developed. Following cracking, the strain becomes more compressive between individual pairs of DEMEC points not intersected by a crack, due to release of tension in the concrete at the cracks. Prior to the development of extensive cracking, adopting a restraint factor of 0.5, as suggested in EC2, greatly overestimates the measured restrained strain.

Cracking is predicted if the restrained strain exceeds the tensile strain capacity of the concrete ε_{ctu}. According to C766, the ratio of the mean tensile strength (f_{ctm}) to the mean elastic modulus (E_{cm}) (depicted "$\varepsilon_{ctu\ EC2}$") provides a lower bound to ε_{ctu} that can be used for design. Section 4.9.2 of C766 (depicted "$\varepsilon_{ctu\ C766}$") accounts for loading duration and creep by multiplying $\varepsilon_{ctu\ EC2}$ by 1.08 at early age (3 days) and 1.40 at "late life" which is taken as $\geq$ 28 days in this paper with linear interpolation between 3 days and 28 days. Both $\varepsilon_{ctu\ EC2}$ and $\varepsilon_{ctu\ C766}$ are plotted in Fig. 11 which shows reasonable correspondence between the actual time of cracking and that predicted from the intersection of the experimentally determined restrained strain and $\varepsilon_{ctu\ C766}$. If checked at 3 days and at EOM, as done in the guidance, C766 correctly predicts wall W1 not to crack and W2 to W12 to crack. However, C766 wrongly predicts cracking at EA in walls W2 to W5, which cracked later. In walls W6 to W12, the risk of cracking is calculated to be very high at EA, with

Table 10
Risk of cracking using EC2-23 and C766.

	EC2-23		C766		Age at first cracking (d)
	EA (3 d)	28 d	EA (3 d)	28 d	
W1	1.6	1.5	1.0	0.7	-
W2	1.5	1.2	1.1	0.8	10.3
W3	1.8	1.4	1.4	0.9	7.3
W4	2.2	1.5	1.7	1.1	19.5
W5	1.9	1.2	1.3	0.8	20.3
W6	3.5	2.6	2.8	1.8	1.14
W7	3.2	2.2	3.0	2.0	1.17
W8	3.1	2.0	2.8	1.9	1.98
W9	2.5	1.9	2.1	1.5	1.91
W10	2.3	1.8	2.1	1.6	1.91
W11	2.8	1.5	2.4	1.5	1.89
W12	3.0	1.7	2.6	1.5	1.85

the predicted time of cracking time close to that observed.

Annex D of EC2–23 expresses the risk of cracking due to restraint, at time t, as $\frac{\sigma_1(t)}{0.8f_{ct,eff}(t)}$ where $\sigma_1(t)$ is the tensile stress in the concrete and $f_{ct,eff}(t)$ is the effective concrete tensile strength, which may be taken as $f_{ctm}(t)$ based on [1]. The maximum tensile stresses to be considered in this assessment are given in Eqs. (14) and (15) below as σ_{1EA} at EA and σ_{1LT} in the LT.

$$\sigma_{1EA} = R_1 \frac{E_c(t_2)}{1+\chi\varphi_{st}} \left(k_{Temp}\alpha_c\left(T_{c,max}-T_0\right) + \left[\varepsilon_{cbs}(t_{crit}) - \varepsilon_{cbs}(t_2)\right]\right) \quad (14)$$

$$\sigma_{1LT} = R_1 \frac{E_{c,28}}{1+\chi\varphi(t,t_2)} \left(k_{Temp}\alpha_c\left(T_{c,max}-T_0\right) + \left[\varepsilon_{cbs}(t) - \varepsilon_{cbs}(t_2)\right]\right) + R_2 E_{c,28}\alpha_c \Delta T_{min} + R_3 \frac{E_{c,28}}{1+\chi\varphi(t,t_s)} \cdot \left[\varepsilon_{cds}(t) - \varepsilon_{cds}(t_2)\right] \quad (15)$$

in which $E_c(t)$ is the concrete elastic modulus at time t, k_{Temp}= 0.9, α_c is the CTE and t_2 is the time at which stress switches from compression to tension at the critical section. Time t_2 was estimated using the three-step method [1] to be around 1 day for the tested walls. The coefficient χ is an aging factor, φ_{st} is a short-term creep factor, $T_{c,max}$ is the peak temperature of hydration and T_0 is the ambient temperature. As recommended in EC2–23, the age adjusted creep coefficient $\chi\varphi_{st}$ was taken as 0.55 and the long-term ageing coefficient χ as 0.8. $\varphi(t,t_2)$ is the summation of basic and drying creep which was determined using Annex B.5 of EC2–23. ΔT_{min} is the change in ambient temperature after the change in restraint factor to R_2.

The stress σ_1 (see Eqs. (14) and (15)) was calculated, as a function of time t, for the tested walls with $R_1 = R_2 = R_3 = 0.5$, $\Delta T_{min} = 0$ and experimentally determined EA thermal strain, shrinkage strain and concrete elastic modulus. Additionally, σ_1 (designated $\sigma_{1expt(\varepsilon_r)}$) was calculated using the maximum measured restrained strain.

Fig. 12 compares stresses σ_1 and $\sigma_{1expt(\varepsilon_r)}$ with 1) $0.8f_{ctm}(t)$ (where $f_{ctm}(t)$ was calculated in terms of the 28-day measured concrete tensile strength using equations B.2 and B.3 from Annex B of EC2–23 (see Eqs. (1) and (2)) and 2) a maturity adjusted concrete tensile strength $f_{ctm,TMC}(t)$ which accounted for the strength development of the TMC cubes. Results are shown for walls W2 to W4, where cracking occurred between 7 and 20 days and W6 which cracked at 1 day. Fig. 12 clearly shows that it is conservative to adopt $R_1 = R_1 = R_3 = 0.5$ in Eqs. (14) and (15) when assessing the risk of cracking in the tested walls. Fig. 12 shows that the stress $\sigma_{1expt(\varepsilon_r)}$ develops more slowly than reality, resulting in the time of first cracking being predicted later than observed in walls W2 and W3 with even the lower bound tensile strength of $0.8f_{ctm}(t)$.

Table 10 evaluates the methodologies proposed by C766 and EC2–23 for estimating the risk of cracking for all 12 walls at EA (3 days) and 28 days. The cracking risk is expressed as $\frac{\sigma_1(t)}{0.8f_{ct,eff}(t)}$ for EC2–23 and $\frac{\varepsilon_r}{\varepsilon_{ctu\ C766}}$ for C766. Where the ratio exceeds 1.0, and cracking was observed in the wall, the cracking prediction is considered accurate and shaded green. When cracking was predicted but not observed, the prediction is considered conservative and shaded blue. If cracking occurred but was not predicted, the cell is shaded red. Table 10 shows EC2–23 to be more conservative than C766, particularly at early age, with the risk of cracking exceeding 1.0 for all the walls, including W1, which did not crack. EC2–23 and C766 wrongly predict cracking at early age (EA) in walls W1 to W5 but correctly predict EA cracking in walls W6 to W12. The C766 cracking risk is lower at 28 days than 3 days due to the tensile strain capacity increasing faster than the restrained strain.

Table 11
Minimum and provided area of steel per m face (mm^2).

	EC2-04		C766		EC2-23		Provided
	EA	LT	EA	LT	EA	LT	
W1	**635**	**763**	352	442	**508**	**611**	436
W2	403	725	217	408	322	580	1117
W3	524	708	282	399	419	567	1117
W4	**563**	**647**	**304**	**364**	**450**	**518**	**262**
W5	**504**	**664**	272	374	403	**531**	436
W6	**436**	**473**	225	255	**348**	**378**	262
W7	317	350	164	189	253	280	436
W8	278	385	144	208	223	308	1117
W9	337	455	174	245	270	364	670
W10	**278**	**455**	**144**	**245**	**222**	**364**	0
W11	231	455	119	245	185	364	1117
W12	**380**	**487**	**202**	**270**	**304**	**389**	0

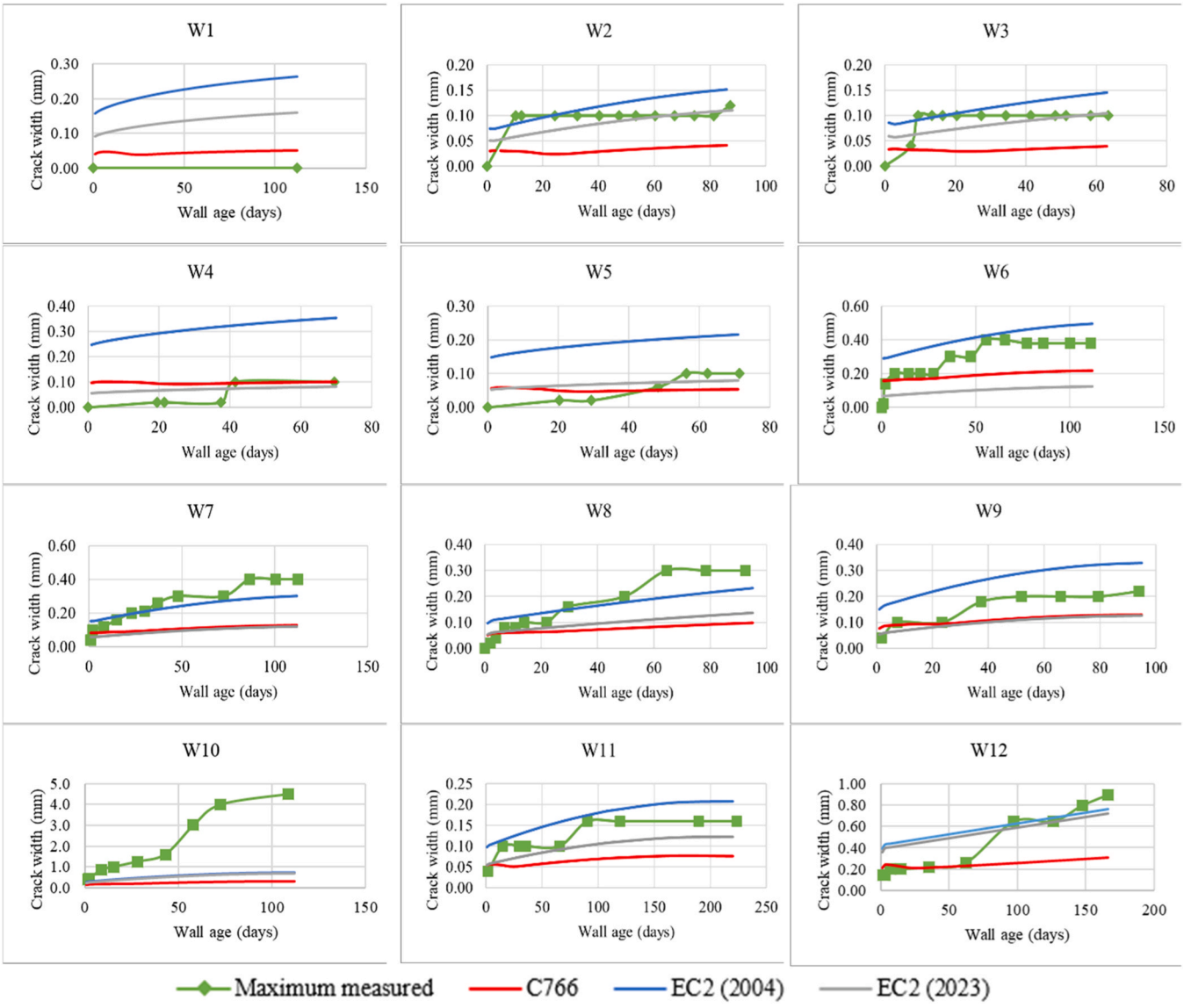

Fig. 13. Comparison of maximum measured and calculated crack widths.

4.3. Minimum area of horizontal reinforcement

In tension members, the tensile resistance of the reinforcement needs to exceed the cracking load to obtain multiple cracking. Accordingly, EC2–04 calculates the minimum area of reinforcement as follows:

$$A_{s,\min\ EC2-04} = k_c.k.f_{ct,eff}.A_{ct} \Big/ \sigma_s \tag{16}$$

in which $f_{ct,eff}$ is the effective tensile strength of concrete at first cracking, A_{ct} is the area of concrete in tension before cracking, and σ_s is the maximum stress permitted in the reinforcement, which may be taken as the characteristic reinforcement yield strength f_{yk}. $k_c = 1$ for pure tension, and k reduces linearly from 1.0 to 0.65 as the section thickness increases from 300 mm to 800 mm. EC2–23 adopts a similar formulation to EC2–04 but replaces $k_c.k$ in Eq. (15) with k_h which is calculated as follows:

$$k_h = 0.8 - 0.6(\min\{b;h\} - 0.3) \geq 0.5 \text{ and } \leq 0.8 \tag{17}$$

in which b and h depict the section width and height in metres.

Consideration of wall W12 shows that multiple cracks can develop in edge restrained walls without horizontal reinforcement due to the restraining effect of the base. C766 acknowledges the restraining effect of the base on cracking by reducing $A_{s,\min}$ from EC2–04 by a multiple $k_{Redge} = 1 - 0.5R$, where R is the edge restraint factor at a height of $h = 0.1L$ above the base. In the calculation of $A_{s,\min}$, C766 reduces $f_{ct,eff}$ to $0.7f_{ctm}$ where f_{ctm} is the mean concrete tensile strength. Table 11 compares the areas of horizontal reinforcement provided in each of the tested walls with the minimum areas required at EA and in the LT by each method.

The minimum reinforcement areas were calculated using the measured concrete tensile strength at 3 days for EA and 28 days for LT. The LT minimum reinforcement requirements govern unless cracking is predicted to occur at EA but not in the LT. The minimum reinforcement area required by C766 ranges between 52 % and 58 % of that required by EC2–04. The minimum area drops by 20 % in EC2–23 compared to EC2–04 since $k_h = 0.8$. The provided area of horizontal reinforcement exceeded or matched that required by C766 in all walls except W4, W10 and W12. The provided area met the requirements of both EC2–04 and EC2–23 in walls W2, W3, W7 to W9 and W11. Values in bold indicate cases where the provided horizontal reinforcement did not meet the required minimum.

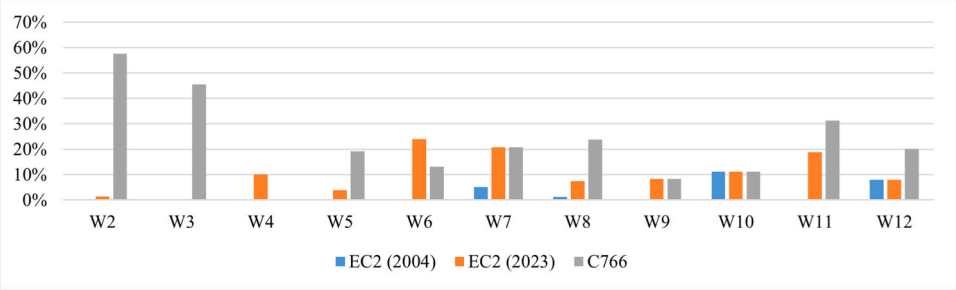

Fig. 14. Percentage of crack width measurements exceeding calculated width at EOM.

4.4. Comparison of measured and calculated EC2-04, C766 and EC2-23 crack widths

Crack widths were calculated with Eqs. (3) and (4) using EC2–04, C766 and EC2–23. EC2–04 and C766 take the crack spacing S in Eq. (3) as:

$$s_{r,\max} = 3.4c + k_1 k_2 k_4 \frac{\phi}{\rho_{p,eff}} \leq 1.3H \tag{18}$$

in which c = cover, $k_1 = 0.8$ for high bond bars, $k_2 = 1$ for direct tension and $k_4 = 0.425$, ϕ is the bar diameter and H is the wall height. The reinforcement ratio $\rho_{p,eff} = A_s/(bh_{c,ef})$ in which A_s is the reinforcement area within width b. For tension members, $h_{c,ef}$ is the lesser of $t/2$ and $2.5\left(c+\frac{\phi}{2}\right)$ where t is the member thickness.

EC2–23 takes S in Eq. (3) as $k_w s_{r,m,cal}$ in which $s_{r,m,cal}$ is the slip length during the crack formation stage and the mean crack spacing when all cracks have formed. For edge restrained walls constrained to remain straight:

$$s_{r,m,cal} = 1.5c + \frac{k_{fl}.k_b}{7.2}\frac{\phi}{\rho_{p,eff}} \leq 1.3H \Big/ k_w \tag{19}$$

in which with $k_{fl} = 1$ for pure tension, $k_b = 0.9$ for good and 1.2 for poor bond conditions and $k_w = 1.7$. The reinforcement ratio $\rho_{p,eff} = 0.25\pi\phi^2/A_{c,eff}$ in which $A_{c,eff} = (\min(s, 10\phi) \times \min(a_x + 5\phi, 3.5a_x, 10\phi, 0.5t)$ where s is the bar spacing and $a_x = c + 0.5\phi$. Non defined notation is as in Eq. (18). EC2–23 states that its calculated crack widths are nominal values that should not be compared with crack widths measured on site.

Crack widths were calculated assuming good bond for walls W1 to W12 in terms of the maximum experimentally determined free strain using EC2–04, C766 and EC2–23. The restraint factor was taken as 0.5 for EC2–04 and EC2–23. The C766 restraint factor was calculated with Eqs. (6) and (7) and then reduced for creep as described above Eq. (10) with linear interpolation between 3 and 28 days. The resulting crack widths are plotted against time in Fig. 13. The calculated crack widths steadily increase with time unlike the measured widths which increase in discrete steps, but this may be due to gaps in time between crack width measurements. C766 is seen to give the least crack width and EC2–04 the greatest. EC2–23 always predicts lower crack widths than EC2–04 because 1) the crack spacing is between 24 % and 75 % less and 2) the peak temperature drop is reduced by a multiple of 0.9. The factor of 0.9 reduces the restrained strains relative to EC2–04 by 10 % at EA and up to 6 % at 100 days. EC2–23 gives greater crack widths than C766 despite the smaller crack spacing due to the higher adopted restraint factor of 0.5. When considering Fig. 13, it is pertinent to note that the design crack width in water retaining and resisting structures is typically limited to 0.2 mm as this is the maximum for autogenous crack healing. More onerous limits can apply to structures like deep basements subject to high water pressures. In this context, it is notable that the measured maximum crack widths in walls W6 to W8 all comfortably exceed 0.2 mm despite the crack widths calculated with C766 and EC2–23 being at most ~0.2 mm and mostly significantly less. On average, EC2–23 performs better than C766 in estimating maximum crack widths but the calculated crack widths are significantly less than measured in walls W6 to W10 which all cracked at EA. Practically, the underestimate of maximum crack width by C766 and EC2–23 is most significant in walls W7 and W8 since the crack width was calculated to be less than 0.2 mm but was 0.4 mm in wall W7 and 0.3 mm in wall W8. EC2–04 gives a conservative estimate of the maximum measured crack width in all walls except W7, W8, W10 and W12. The percentage of EOM crack width measurements exceeding the calculated value was determined for each wall using the data in Table 8. The results are shown in Fig. 14 where C766 is seen to underestimate crack widths in all walls except W4, with the percentage of measurements being underestimated in each wall ranging from 8 % to 58 %. The percentage of measurements exceeding the calculated width increases significantly if only through cracks are considered. On average, EC2–23 provides better estimates of crack width than C766 if R is taken as 0.5, with only 9 % of the total number of crack widths measured in all walls being greater than calculated. In the case of EC2–04, only 2 % of the total number of crack widths measured in all walls were greater than calculated compared with 25 % for C766.

4.5. Discussion

Prior to the development of significant cracking the experimentally determined restrained strain was closest to that calculated with C766. Furthermore, as shown in Table 10, C766 predicts cracking in all the walls as observed. The C766 method is considerably simpler to use than that in EC2–23 and is therefore recommended. Following cracking, the experimentally determined restrained strain increased substantially due to the measured surface strain becoming less compressive, or tensile, between pairs of adjacent DEMEC points that were crossed by cracks. At EOM, the maximum experimentally determined restrained strains in walls W2, W6, W7, W8, W9, W11 and W12 were reasonably close to those calculated using a restraint factor of 0.5 (see Fig. 11). EC2–04 gives the best overall estimate of maximum crack width in these walls. EC2–23 gives lower crack widths than EC2–04 primarily due to the calculated crack spacing being less. C766 significantly underestimates the maximum measured crack widths due to the calculated restrained strain at EOM being significantly less than measured.

The tests show that the mean measured restrained strain increases significantly following cracking, due to localised tensile strain increments across cracks. Consequently, reducing the restraint factor by a creep factor, as done in C766, is justified for assessing risk of cracking but not for the calculation of crack width in edge restrained walls with EC2. Rather, adoption of a simplified restraint factor of 0.5 is recommended for crack width calculation in edge restrained walls as permitted by EC2.

It should be noted that the behaviour of the walls depends on localised variations in thermal and shrinkage strains and material properties. The effect of such variations could in theory be investigated

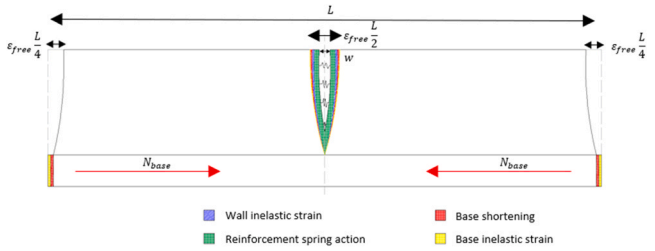

Fig. 15. Components of crack width calculations in reinforced walls.

numerically with a suitable model but in practice, the intention of the design codes is to limit the maximum calculated crack width to a specified value. This is done by calculating a maximum crack width with typically a 5 % chance of being exceeded. Hence, the code design equations already make allowance for the variability in material properties. In our opinion, the inaccuracies in the code equations result from the cracking behaviour of the walls being more complex than assumed in the derivation of the code equations as discussed below.

4.6. Development of simplified design model

As shown in Section 4, EC2–04, C766 and EC2–23 adopt similar methods for the calculation of crack width in edge restrained walls. The main differences lie in the calculation of crack spacing and restraint factor. Of the three methods EC2–04 gives the best estimates of maximum crack width in the tested walls. However, none of the three methods properly capture the response of the walls after cracking. This is due to the models unrealistically 1) calculating the restrained strain at EOM assuming the member is uncracked and 2) taking the crack spacing as that in a tie in which stabilized cracking has developed [16].

The basis of a more realistic design model can be seen in the behaviour of walls W10 and W12, without horizontal reinforcement. The response of W10, with aspect ratio L/H = 5.1, was dominated by the early age formation of a single full height vertical through crack near the centre of the wall. This crack divided the wall in two leading to a reduction of restraint in each half. Over the remainder of the monitoring period, the initial crack widened significantly but only fine surface cracks, of no practical consequence, formed elsewhere in the wall. In wall W12, with L/H = 4.0, three vertical cracks formed at early age, with spacing approximately equal to the wall height, dividing the wall into four sections of similar length. As in wall W10, subsequent cracking was minimal. Only one of the three EA cracks in wall W12 extended over the full height of the wall. This crack was significantly wider than the other two EA cracks as shown in Fig. 7, due to the restraining effect of the concrete bridging over the partial height cracks. In walls W6 and W7 with 0.3 % and 0.5 % horizontal reinforcement respectively, the key influence of reinforcement was to limit the maximum width of the initial EA cracks to 0.4 mm over the whole monitoring period compared with a maximum of 4.5 mm in wall W10. The behaviour of walls W8 and W9 with 1.3 % and 0.8 % reinforcement respectively differed from walls W6 and W7 in that additional through cracks developed within the first month. Additionally, more fine surface cracks formed in walls W8 and W9 compared with walls W6 and W7. The maximum crack width was unexpectedly greater in wall W8 with 1.3 % horizontal reinforcement than W9 with 0.8 % reinforcement demonstrating the random nature of cracking.

The observed behaviour provides insights into the mechanics of cracking in thin base restrained walls as illustrated in Fig. 15, where the horizontal reinforcement is represented by a series of springs. In the absence of restraint from horizontal reinforcement, an upper bound to the maximum crack width (see Fig. 15) is given by:

$$w_{unreinforced} < \varepsilon_{free}\frac{L}{2} \tag{20}$$

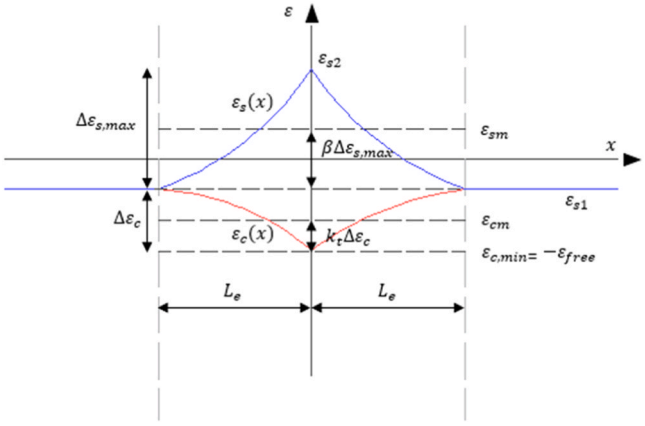

Fig. 16. Strain diagram in reinforced concrete tie during single cracking stage due to shrinkage and axial load.

where ε_{free} is the differential free strain between the wall and base.

Following cracking, tension develops in the reinforcement which reduces the crack width below $w_{unreinforced}$ as well as reducing the increment in free strain needed to form additional cracks. For $\frac{L}{H} \geq 4$, second and third full height cracks are assumed to form simultaneously at a distance H from the wall centreline when the maximum average tensile stress, over the wall height, to either side of the first crack reaches the concrete tensile strength. The crack width is estimated as:

$$w = \varepsilon_{free} S(1 - \frac{\rho_h \sigma_{s2}}{\sigma_r}) \geq 0 \tag{21}$$

where $\varepsilon_{free} = \alpha T_1 + \varepsilon_{sh}$ is the free strain, S is the crack spacing which is taken as $0.5L$ for a single crack, and the wall height H otherwise, $\rho_h = A_{sh}/A_c$ is the horizontal reinforcement ratio and σ_{s2} is the reinforcement stress at the crack. σ_r is the mean tensile stress induced over the height of an uncracked wall of length L^*, at its centreline, by restraint of ε_{free}. The length of wall L^* considered in the calculation of σ_r is $L^* = L$ for 1 full height crack and $L^* = 0.5L$ for 3 full height cracks which is the maximum considered in the present analysis. The term $\frac{\rho_h \sigma_{s2}}{\sigma_r}$ equals the ratio of the average stress induced in the concrete by the reinforcement to σ_r which can be estimated as:

$$\sigma_r = E_{c,ef} R_{ave} |\varepsilon_{free}| \tag{22}$$

in which $E_{c,ef} = K_c E_{cm}$ in which K_c is a creep factor which according to [2] can be taken as 0.65 at EA (3 days) and 0.5 in the LT. R_{ave} is the average restraint factor over the height of a wall of length L^* at its centreline, which can be determined with elastic FEA or Eqs. 6 and 7 from C766.

During the crack formation stage, the reinforcement strain varies to either side of cracks as shown in Fig. 16. Making the simplifying assumption that the CTE is the same for reinforcement and concrete, the crack width corresponding to the strain distribution in Fig. 16 is given by:

$$w = 2l_e(1 - k_t)(\varepsilon_{s2} + |\varepsilon_{sh}|) \tag{23}$$

in which k_t is a coefficient which can be taken as 0.4 in the long-term [15]. Consideration of equilibrium gives:

$$l_e = \frac{\phi}{4}\frac{\Delta\sigma_s}{\tau} = \frac{\phi}{4\tau}\frac{(\varepsilon_{s2} + |\varepsilon_{sh}|)E_s}{1 + m\rho_h} \tag{24}$$

in which $\Delta\sigma_s$ is the change in reinforcement stress over l_e, $m = \frac{E_s}{E_{c,eff}}$ is the modular ratio, ε_{s2} is the reinforcement strain at the crack, E_s is the reinforcement elastic modulus and $E_{c,eff} = \frac{E_c}{1+\phi}$ where ϕ is the creep co-

Table 12
Calculated and maximum measured crack widths (mm) in walls with EA through cracks.

Wall	Calculated crack width (mm)						Calc/Expt	
	W6	W7	W8	W9	W10	W12	Mean	St. Dev.
Experimental	0.38	0.40	0.30	0.22	3.0	0.9	-	-
Proposed	0.48	0.41	0.24	0.33	2.6	1.14	1.12	0.27
EC2–06	0.5	0.3	0.25	0.33	0.73	0.76	0.92	0.45
EC2–23	0.12	0.12	0.15	0.13	0.71	0.73	0.45	0.21
C766	0.22	0.13	0.11	0.13	0.29	0.30	0.38	0.18

efficient. $E_{c,eff}$ is taken as $0.5E_c$ in the present analysis for consistency with C766. Substituting for l_e in Eq. 23 and assuming the average bond stress $\tau = 1.8f_{ctm}$ [30] gives:

$$w = \frac{\phi E_s}{6f_{ctm}} \cdot \frac{(\sigma_{s2}/E_s + |\varepsilon_{sh}|)^2}{1 + m\rho_h} \tag{25}$$

The crack width can be calculated in terms of the differential free strain between the wall and base ε_{free} and the number of cracks by simultaneously solving Eqs. (21) and (25). The restraint factor R_{ave} in Eq. (22) reduces each time further cracks form. For the tested walls, R_{ave} is estimated from Eqs. (6) and (7), using a creep factor of 0.5, to be 0.25 for 1 crack and 0.18 for 3 cracks.

The behaviour modelled above is similar to that of walls W6, W7 and W12, with $\rho_h = 0.3\%,\ 0.5\%$ and 0 % respectively, in which three full, or near full height, through thickness cracks formed with spacing approximately equal to the wall height. According to the simplified model described above the crack widths at EOM in walls W6, W7 and W12 are 0.48 mm, 0.41 mm, and 1.14 mm which compare favourably with the measured values of 0.38 mm, 0.40 mm and 0.90 mm. If calculated assuming one crack, the estimated crack width in wall W10 is 2.6 mm which compares well with the measured crack width of 3 mm at the top of the wall. The model is less applicable to walls W8 and W9 which were more heavily reinforced with $\rho_h = 1.3\%$ and $\rho_h = 0.8\%$ respectively where many cracks formed. Even so, the model gives reasonable estimates of measured crack width of 0.24 mm for W8 and 0.33 mm for wall W9 compared with measured values of 0.30 mm and 0.22 mm respectively. Table 12 shows that the proposed method gives considerably more accurate estimations of crack width in the walls that developed through cracks at EA than C766 and EC2–23. The predictions also compare favourably with those obtained using EC2–06.

5. Conclusions

The paper describes an experimental campaign in which 12 large scale reinforced concrete walls were cast onto reinforced concrete bases to study the development of EA thermal and LT cracking in edge restrained walls. Variables included the concrete mix design, wall aspect ratio and reinforcement arrangement. Detailed measurements were made of concrete properties, temperature, strain and crack width. Two walls had no horizontal reinforcement. The initial EA crack pattern was similar in walls without and with horizontal reinforcement. The subsequent behaviour diverged with reinforcement controlling the deformation of the wall to either side of cracks and, hence, the crack width. Tension in the reinforcement at the cracks also reduced the loss of restraint in the concrete due to cracking, thereby enabling other cracks to form with increasing free strain.

The risk of cracking was assessed for the tested walls using the approaches of C766 and EC2–23. C766 assesses the risk of cracking by comparing the restrained strain with the tensile strain capacity of concrete while EC2–23 compares the tensile stress induced by restraint with the concrete tensile strength. The C766 approach was found to be simplest and most accurate particularly if the assessment was made using the experimentally derived restrained strain.

Comparisons were made between measured crack widths and crack widths calculated with EC2–04, EC2–23 and C766 using the measured free strain. In this, the restraint factor was taken as 0.5 in EC2–04 and EC2–23, as recommended, but calculated in terms of wall geometry for C766 with a further reduction being made for creep. EC2–04 was found to give the most realistic estimates of maximum crack widths in walls that cracked at EA (W6 to W12) but to overestimate crack widths in other walls (W1 to W5). C766 significantly underestimated the measured maximum crack widths in almost all walls largely due to the reduction in restraint factor for creep. Crack widths calculated with EC2–23 typically lie between those calculated with EC2–04 and C766.

Based on the experimental observations, a simplified mechanical model is presented for calculating crack widths in edge restrained walls. The model accounts for the interaction between horizontal reinforcement and the basic crack pattern that develops in walls without horizontal reinforcement due to base restraint. The model is shown to give better estimates of maximum crack width in the walls that cracked at EA than EC2–04, C766 and EC2–23.

CRediT authorship contribution statement

Karim El Khoury: Writing – original draft, Project administration, Methodology, Investigation, Formal analysis, Data curation. **Bassam Izzuddin:** Writing – review & editing, Supervision, Funding acquisition. **Vollum Robert Lars:** Writing – review & editing, Supervision, Project administration, Funding acquisition, Conceptualization. **John Forth:** Writing – review & editing, Investigation, Funding acquisition, Conceptualization.

Declaration of Competing Interest

The authors declare that they have no known competing financial interests or personal relationships that could have appeared to influence the work reported in this paper.

Acknowledgements

The authors kindly acknowledge financial support from the Engineering and Physical Sciences Research Council (EPSRC) under grants EP/T004142/1 and EP/T004185/1 titled Understanding the cracking behaviour of reinforced concrete elements subjected to the restraint of imposed strains.

Notation

Notation - Uppercase Symbols	Definition	Dimensions
A_{base}, A_{old}	Area of the base or restraining element	L^2
A_{wall}, A_{new}	Area of the wall or newly cast element	L^2
A_{ct}	Area of concrete in tension	L^2
A_s, $A_{s,min}$	Area or minimum area of steel reinforcement	L^2
E_c, $E_c(t)$, $E_{c,28}$	Elastic modulus of concrete (at time t or 28 days)	$ML^{-1}T^{-2}$
E_{cm}	Mean modulus of elasticity of concrete	$ML^{-1}T^{-2}$
$E_{c,eff}$	Effective elastic modulus of concrete including creep	$ML^{-1}T^{-2}$
$E_{c,min}$	Minimum modulus of elasticity of concrete	$ML^{-1}T^{-2}$

(*continued on next page*)

(*continued*)

Notation - Uppercase Symbols	Definition	Dimensions
E_s	Modulus of elasticity of steel reinforcement	$ML^{-1}T^{-2}$
$f_{cm}, f_{cm}(t)$	Mean compressive strength of concrete (at 28 days or time t)	$ML^{-1}T^{-2}$
$f_{ctm}, f_{ctm}(t), f_{ctm,TMC}$	Mean or maturity-adjusted tensile strength of concrete	$ML^{-1}T^{-2}$
$f_{ct,eff}$	Effective tensile strength of concrete at cracking	$ML^{-1}T^{-2}$
H, H_w	Wall height	L
L, L_w	Wall length	L
$R, R_j, R_{ave}, R_{1/2/3}$	Restraint factor (general or code-specific)	–
$s_{r,max}, s_{r,m,cal}$	Maximum or mean calculated crack spacing	L
$T, T_0, T_1, T_2, T_{c,max}$	Temperature variables (ambient, peak, differential, etc.)	Θ
$w, w_{unreinforced}$	Crack width (reinforced or unreinforced cases)	L

Notation - Lowercase Symbols	Definition	Dimensions
α, α_c	Strength development or thermal expansion coefficient	– / ε/°C
ΔT	Temperature difference	Θ
ε_{free}	Free strain	–
$\varepsilon_{sh}, \varepsilon_{cs}$	Shrinkage strain	–
ε_{th}	Thermal strain	–
$\varepsilon_r, \varepsilon_{rest,max}$	Restrained strain	–
$\varepsilon_m, \varepsilon_{meas}$	Measured or developed strain	–
$\varepsilon_{cm}, \varepsilon_{sm}$	Mean concrete strain or mean strain in reinforcement	–
ε_{ctu}	Tensile strain capacity of concrete	–
ε_{s2}	Steel strain at crack	–
$\varepsilon_{ca}, \varepsilon_{cd}$	Autogenous and drying shrinkage strains	–
$\varepsilon_{cbs}(t), \varepsilon_{cds}(t)$	Shrinkage strain components as defined in EC2–23	–
$\Delta\varepsilon$	Localised strain increment due to cracking	–
$\sigma_{ct}(t)$	Concrete tensile stress at time t	$ML^{-1}T^{-2}$
σ_s, σ_{s2}	Reinforcement stress (general or at crack)	$ML^{-1}T^{-2}$
σ_r	Restraint-induced stress in concrete	$ML^{-1}T^{-2}$
φ	Reinforcement bar diameter	L
$\rho_h, \rho_v, \rho_{p,eff}$	Reinforcement ratios (horizontal, vertical, effective)	–
τ	Average bond stress	$ML^{-1}T^{-2}$
$\chi, \varphi(t, t_x)$	Ageing and creep coefficients	–
$k, k_c, k_t, k_h, k_b, k_{fl}, k_w, k_{Temp}, k_{Redge}$	Empirical coefficients from codes	–
M	Modular ratio (E_s / E_c,eff)	–
l_e	Effective anchorage or transfer length	L
$\beta_{cc}(t)$	Strength development coefficient for compression	–

Data availability

Data will be made available on request.

References

[1] Bjøntegaard Ø. COIN project report no. 31: basis for and practical approaches to stress calculations and crack risk estimation in hardening concrete structures – state of the art (Blindern) Nor Public Roads Adm 2011. ⟨www.coinweb.no⟩ ([Online]. Available).

[2] P. Bamforth, *Control of Cracking Caused by Restrained Deformation in Concrete (CIRIA Report C766),* CIRIA, London, 2018.

[3] Azenha M, Kanavaris F, Jędrzejewska A, et al. Recommendations of RILEM TC 287-CCS: Thermo-Chemo-Mechanical modelling of massive concrete structures towards cracking risk assessment. Mater Struct Mater Et Constr Aug. 2021;54(4). https://doi.org/10.1617/s11527-021-01732-8.

[4] Gilbert RI. Cracking caused by Early-Age deformation of concrete – prediction and control. Procedia Eng 2017;172:13–22. https://doi.org/10.1016/j.proeng.2017.02.012.

[5] Nejadi S, Gilbert I. Shrinkage cracking and crack control in restrained reinforced concrete members. Acids Struct J 2004;101(S83):840–5.

[6] Micallef M, Vollum RL, Izzuddin BA. Cracking in walls with combined base and end restraint. Mag Concr Res Nov. 2017;69(22):1170–88. https://doi.org/10.1680/jmacr.17.00026.

[7] P. Bamforth, Concreting Large-Volume (Mass) Pours (CIRIA Publication R135, Ch. 13), CIRIA, London, 1995.

[8] Micallef M, Vollum RL, Izzuddin BA. Crack development in transverse loaded Base-Restrained reinforced concrete walls. Eng Struct Jul. 2017;143:522–39. https://doi.org/10.1016/j.engstruct.2017.04.035.

[9] Jędrzejewska A, Kanavaris F, Zych M, et al. Practical insights on standardised models for estimation of crack width due to imposed strains in Edge-Restrained reinforced concrete elements. Eng Struct Apr 2024:305. https://doi.org/10.1016/j.engstruct.2024.117757.

[10] Schlicke D, Matiašková L. "Advanced computational methods versus analytical and empirical solutions for determining restraint stresses in Bottom-Restrained Walls,". J Adv Concr Technol 2019;17:335–49. https://doi.org/10.3151/jact.17.6.335.

[11] H. Stoffer, *Cracking Due to Shrinkage and Temperature Variations in Walls,* Heron, Issue 3 of 23, Stevin Laboratory, Delft University of Technology and I.B.B.C. Institute TNO for Building Materials and Building Structures, 1978.

[12] Schlicke D, Dorfmann EM, Fehling E, Tue NV. Calculation of maximum crack width for practical design of reinforced concrete. Civ Eng Des Jun. 2021;3(3):45–61. https://doi.org/10.1002/cend.202100004.

[13] BSI, *BS EN 1992–1-1:2004+A1:2014. Eurocode 2: Design of Concrete Structures, Part 1–1: General Rules and Rules for Buildings,* 2014.

[14] BSI, *BS EN* 1992–3:2006. Eurocode 2: Design of Concrete Structures, Part 3: Liquid Retaining and Containment Structures, 2006.

[15] BSI, *BS EN* 1992–1-1:2023. Eurocode 2: Design of Concrete Structures, Part 1–1: General Rules for Buildings, Bridges and Civil Engineering Structures, 2023.

[16] Jędrzejewska A, Zych M, Kanavaris F, et al. Standardized models for cracking due to restraint of imposed strains – the state of the art. Struct Concr Aug 2023;24(4):5388–405. https://doi.org/10.1002/suco.202200301.

[17] ACI Committee 207, *Effect of Restraint, Volume Change and Reinforcement of Cracking of Mass Concrete,* 207.2R–95, American Concrete Institute, 2002.

[18] ACI Committee 224, *Control of Cracking in Concrete Structures*, American Concrete Institute, 2001.

[19] Shehzad MK, Forth JP, Bradshaw A. Imposed loading effects on reinforced concrete walls restrained at their base. Proc Inst Civ Eng Struct Build Jun. 2020;173(6):413–28. https://doi.org/10.1680/jstbu.17.00179.

[20] Jędrzejewska A, Kanavaris F, Zych M, Schlicke D, Azenha M. Experiences on early age cracking of Wall-on-Slab concrete structures. Structures Oct. 2020;27:2520–49. https://doi.org/10.1016/j.istruc.2020.06.013.

[21] Elwakeel A, Shehzad M, El Khoury K, et al. Assessment of cracking performance in edge restrained RC walls. Struct Concr Jun. 2022;23(3):1333–52. https://doi.org/10.1002/suco.202100688.

[22] Menga A, Torrenti J, Kanstad T, Klausen ABE. Early-Age cracking due to restraint: laboratory and field investigations on the predictive capacity of the simplified method in Annex D of the future EC2. Struct Concr Dec. 2024;25(6):4300–23. https://doi.org/10.1002/suco.202400173.

[23] Property Care Association, *Best Practice Guidance – Type B Waterproof Systems (BS 8102:2022)*, Huntingdon, UK, 2022. [Online]. Available: ⟨https://www.property-care.org/resources/best-practice-guidance-type-b-waterproofing-systems⟩.

[24] El Khoury K, Ridley I, Vollum R, et al. Experimental assessment of crack prediction methods in international design codes for edge restrained walls. Structures Sep. 2023;55:1447–59. https://doi.org/10.1016/j.istruc.2023.06.087.

[25] BSI, BS EN 12390-3:2009. *Testing Hardened Concrete. Part 3: Compressive Strength of Test Specimens*, 2011.

[26] BSI, BS EN 12390-13:2013. *Testing Hardened Concrete. Part 13: Determination of Secant Modulus of Elasticity in Compression*, 2013.

[27] El Khoury K. Cracking in Edge Restrained Concrete Walls. London, UK: Imperial College; 2024. PhD thesis.

[28] Elwakeel A, Shehzad M, El Khoury K, et al. Understanding the Cracking Behaviour of Reinforced Concrete Elements Subjected to the Restraint of Imposed Strains. Lisbon 2021.

[29] T. Kanstad, A. Klausen, and A. Menga, *Background Document to prEN1992-1-1 D7 Rev 7 Annex D: Evaluation of Early-Age and Long-Term Cracking Due to Restraint*, Norway, 2021.

[30] Schlicke D, Tue NV, Gomes J, Sousa C, Azenha M. Analytical assessment of restraint forces and crack widths in End-Restrained building slabs. Eng Struct Dec. 2020;224:111218. https://doi.org/10.1016/j.engstruct.2020.111218.